LUT University
LUT School of Energy Systems
LUT Mechanical Engineering

Arvo Niini

ADDITIVE MANUFACTURING OF THREAD CUTTING TOOL

Updated 03.06.2019

Examiner(s): Professor Juha Varis
M. Sc. (Tech.) Adam Kazmierczak

TIIVISTELMÄ

LUT-yliopisto
LUT School of Energy Systems
LUT Kone

Arvo Niini

Kierretyökalun additiivinen valmistus

Diplomityö

2019

75 sivua, 73 kuvaa, 7 taulukkoa, 2 yhtälöä ja 6 liitettä

Tarkastajat: Professori Juha Varis
DI Adam Kazmierczak

Hakusanat: Additiivinen valmistus, kierretapit, kierteitysmomentti, topologia optimointi

Tutkimuksen tavoite oli M16 kierretapin valmistelu additiiviseen valmistukseen tehtiin suunnittelu- ja topologia optimoinnin muodossa aikomuksena kokeellinen kierteitystehon vahvistus hybridivalmisteiselle M16 kierretapille, jossa optimoitu kierretapin pää olisi yhteenliitettynä perinteisesti valmistetun kierretapin varren kanssa kitkahitsauksen avulla. Kierretapin lastu-uran nousukulman, rintakulman, viisteen kulman ja viisteen pituuden vaikutuksia M16 kierretapin pään poikkileikkauksien jännitysjakaumaan tutkittiin suunnitteluoptimoinnissa ennen niiden optimaalisten arvojen valintaa. Topologia optimoinnin vaatimukset kierretapin päälle esitettiin sekä sisäisten ympyrä, neliö, viisikulmio ja kuusikulmio verkkorakenteiden sekä sisäisen onton rakenteen vaikutukset kierretapin pään jännitysjakaumaan tutkittiin topologia optimoinnissa. 3D tulostustulokset esitettiin kierretapin pään topologia konfiguraatioilla, jotka oltiin valittu riippuen niiden materiaalikäytön vähennyskyvystä sekä rasitusarvoista kierretapin pään poikkileikkauksilla.

Tätä seurasi kokeellisten kierteityssuoritustestien suorittaminen vakio M16 kierretapeilla. Kokeelliset kierteitystestit tehtiin 35 kulmaisilla spiraaliuraisella vakio M16 kierretapilla ja spiraalikärkisellä vakio M16 kierretapilla alumiini ja ruostumaton teräs työkappaleille. Kierteitystestien tulokset osoittivat kierteitysmomentin laskevan lastuamisnopeuden noustessa. Kierteitystesteistä kerätty laskennallinen malli osoitti vain pientä poikkeamaa kokeellisesti mitatun kierteitysmomentin ja työssä käytetyn numeerisen simulaation kierteitysmomentin välillä. Kokeellisten kierteitysmomenttien tulokset erilaisille vakio kierretappi tyypeille osoitettiin olevan sopusoinnussa aiemman tutkimuksen kanssa.

ABSTRACT

LUT University
LUT School of Energy Systems
LUT Mechanical Engineering

Arvo Niini

Additive manufacturing of thread cutting tool

Master's Thesis

2019

75 pages, 73 figures, 7 tables, 2 equations and 6 appendices

Examiners: Professor Juha Varis
M. Sc. (Tech.) Adam Kazmierczak

Keywords: Additive manufacturing, taps, tapping torque, topology optimization

Preparation of M16 thread tap for additive manufacturing was done in the form of design and topology optimization with intention of experimental tapping performance validation for a hybrid manufactured M16 tap in which optimized tap crown was to be joined with a conventionally manufactured tap shank. Tap flute lead angle, rake angle, chamfer angle and chamfer length were studied in the design optimization in terms of their effect on M16 tap crown stress distribution before selecting their optimal values. Topology optimization requirements for tap crown were detailed in addition to studying how internal circle, square, hexagon and pentagon grid structures as well as internal hollow structure affected tap crown stress distribution in the topology optimization. 3D printing outcomes for tap crown topology configurations chosen based on their tap mass reduction capability and tap crown cross sectional stress distribution were displayed, followed by experimental tapping performance tests with standard M16 taps.

Experimental tapping tests were done with 35° spiral fluted standard M16 tap and straight fluted spiral point standard M16 tap on aluminum and stainless-steel workpieces. Tapping test results showed decrease in measured tapping torque when cutting speed was increased. Derived statistical model from the tapping tests displays relatively small deviation between experimentally measured tapping torque and tapping torque used in numerical simulation of this study. Experimental tapping torque results for different standard M16 tap types were found to be correctly aligned with previous research.

ACKNOWLEDGEMENTS

I would like to express my gratitude for all the guidance and cooperation provided to me by Professor Juha Varis, you have truly enabled such an international thesis project between Finland and Denmark to occur in the first place. I would also like to express my great admiration for all the staff of Thürmer Tools, for allowing my return to the company as a thesis worker even after having already worked there as an Erasmus trainee in the summer of 2018. Likewise, without consultation from the company R&D Engineer Adam Kazmierczak I can honestly doubt whether this thesis project could have moved forward. Lastly, I wish to acknowledge all the immeasurable support I have gotten from home as my home will be there wherever you were, you are, or you will be – Lin.

Arvo Niini
Gilleleje, Denmark 31.05.2019

TABLE OF CONTENTS

LIST OF SYMBOLS AND ABBREVIATIONS

λ	Flute lead angle [deg]
D	Helix diameter [mm]
F	Tapping force [N]
L	Helix pitch [mm]
M	Tapping torque [Nm]
r	Distance from axis of rotation [m]
v_c	Cutting speed [m/min]

ABS	Acrylonitrile butadiene styrene
Al	Aluminum
AM	Additive Manufacturing
CAD	Computer-aided design
CNC	Computer numerical control
DAQ	Data acquisition system
EBM	Electron beam melting
FEA	Finite element analysis
FEM	Finite element method
HSS	High-speed steel
ISO	International Organization for Standardization
LMD	Laser metal deposition
TiN	Titanium nitride
SLM	Selective laser melting
SME	Small and medium-sized enterprises
SS	Stainless-steel

1 INTRODUCTION

1.1 Project background

Studied thesis topic is part of a R&D project undertaken by a Danish family-owned thread cutting tool manufacturer and wholesaler, Thürmer Tools. Thürmer Tools or Thurmer as commonly denoted has a long history of being one of the forerunners in the industry, with founder of Thurmer having invented square threading die already back in 1897. (Thurmer 2019.) Today Thurmer is once again embracing new frontiers of industry by investigating thread cutting tool production opportunities from additive manufacturing as an objective of the ongoing R&D project this thesis work will assist in advancing.

Idea behind the undertaken R&D project of Thurmer is to 3D metal print crown of a thread cutting tap and to attach it with conventionally manufactured tap shank by friction welding. 3D printing the tap crown enables use of optimized tap design for reduction of tap material usage and production time. Reducing material usage and shortening production time via hybrid manufacturing by means of additive manufacturing and conventional machining has potential of making thread cutting tap production more economical, effective and sustainable. From a successful R&D project outcome, Thurmer can expect to offer a superior product into the thread cutting tool markets.

Thesis project consists of smaller individual task items as part of a larger industrial R&D project described above. The task items are design and topology optimization of M16 x 2 HSS (high-speed steel) T15 tap crown for 3D printing, and experimental tapping performance tests. The tapping tests for the 3D printed and post-processed tap crown samples are done after they have been attached to the conventionally manufactured tap shanks by friction welding. Preceding both tap crown optimization and tapping tests, a literature review is conducted to study relevant theoretical aspects of this thesis work.

1.2 Project scope and objective

The tap crown design optimization involves altering of flute lead angle, rake angle, chamfer angle and chamfer length to compare their effect on stress distribution along 3 tap crown cross sections. Altering flute (lead) angle, rake angle, chamfer angle and chamfer length is done in consecutive order, as switching the order would affect optimization results. Consecutive order of tap parameters is decided in terms of priority for altering the parameters, with flute angle being most prioritized and chamfer length least. Priority is due to scale of impact on tap crown stress distribution.

The tap crown topology optimization involves comparing circle, square, pentagon, hexagon and hollow internal structures on their effect on stress distribution along 3 tap crown cross sections, and their tap crown material reduction capability. Designing internal structures in tap crown topology optimization is restricted by 3D printability, preservation of tapping performance, tolerances for friction welding of tap crown with tap shank, margins with tap crown exterior to avoid interference with external thread geometry of the tap and lastly enabling of metal powder release from topology optimized internal geometry after 3D printing.

A simplified 3D finite element tapping model is compiled for design and topology optimization of the tap crown. Tapping simulation in this utilized numerical model is simplified with tapping torque applied upon tap shank while tap cutting edges are fixed. Tap crown stress distribution is measured additionally from 3 cross sections of tap crown for indicators of reflective stress values due to high stress concentration on cutting edges. Tapping simulation is limited to its simplified form to avoid excessive computation time of more reflective tapping models.

Tapping performance will be tested by measuring tapping torque of the 3D printed tap crowns joined with conventionally manufactured tap shanks while altering cutting speed whilst tapping aluminum and stainless-steel workpieces. Additive manufacturing of optimized tap crowns is done by a third party and R&D project partner of Thurmer's. Friction welding and post-processing of the optimized tap crowns with conventionally manufactured tap shanks is likewise done by a third party.

Literature review will focus on additive manufacturing in context of thread cutting tools. Important concepts and definitions to cutting tools, taps and additive manufacturing are laid out. Examples of 3D printed cutting tools in literature are showcased. Relation of finite element method in tapping simulations is discussed and relevant previous finite element tapping simulations studies are introduced to form a theoretical background for the utilized numerical model in this study. The literature review is narrowed to relevant concepts, definitions and examples of additive manufacturing, thread cutting tools and finite element method as it only relates to context and content of the thesis work.

The objective of the study was that by the end of the thesis an optimized thread tap crown had been developed from design to an additive manufactured prototype which had been tapping performance tested after being joined with a conventionally manufactured tap shank. Tapping performance test results would have validated whether the tap crown design and topology optimization had accomplished to reduce tap material usage whilst providing satisfactory tapping performance.

1.3 Research methods

A systematic collection of literature is done by utilizing scientific databases for search of academic publications, industrial handbooks and manuals. Numerical method in the form of finite element analysis is utilized with 3D tapping simulations of optimized tap crowns in their design and topology optimization using SOLIDWORKS software. Tapping performance tests are conducted experimentally with use of ECO.100/4 D magnetic drilling machine, Jiuwu JJCP078 50 kg load cell sensor for measuring tapping torque as well as PLX-DAX add-on for Microsoft Excel to collect results.

Found literature is evaluated from search queries in used scientific databases by subject area, publication year and relevance to thesis topic. Citation indicators will be used when possible to evaluate journals of the found scientific papers given lack of sources. Tapping and taps are under-researched and as such sources are scarce to begin with. Finite element model accuracy of the optimized taps is validated by comparing the simulation results with those of standard taps and by using as fine meshing as possible given hardware and software resources.

Statistical and regression analysis will be conducted on results from tapping performance tests to better describe relationships and correlations among the studied performance parameters. Results of the tapping tests with optimized hybrid manufactured taps will be compared to results with conventionally manufactured standard taps. Tapping tests will be repeated with 10 tapped through holes by each tap on aluminum and stainless-steel workpieces. Statistical model depicts how cutting speed affects tapping torque of the tested taps when tapping aluminum and stainless-steel workpieces.

Research questions of thesis work consist of main research question together with related sub-questions. The main research question and related sub-questions seek answers to what benefits and shortfalls does additive manufacturing of optimized thread tap crown provide. The questions are listed next, with the main research question being:

- Can additive manufacturing enable use of optimized thread cutting tap crown design with reduced material usage and satisfactory tapping performance?

Sub-questions related to main research question are:

- How design of an optimized tap crown differs from a standard one?
- What are the requirements for topology optimization of a tap crown design for additive manufacturing?
- How tapping performance parameters are affected by additive manufactured tap crown?

1.4 Additive manufacturing

Additive manufacturing (AM) is a manufacturing process in which parts are made by joining printing material from the part 3D models typically layer by layer. 3D printing is synonymous with additive manufacturing, albeit providing a more technical context for it. Additive manufacturing process involves use of a 3D printer, which is a machine that is utilized in additive manufacturing. Additive manufacturing can occur in a single-step process where the part is made in one operation which results both in desired shape and material properties of the part. AM can also occur in a multi-step process where the part is made in two or more operations with these subsequent operations being typically required for reaching desired material properties of the part. (ISO/ASTM 52900:2015 2019.)

Application of additive manufacturing from industrial standpoint is common in rapid prototyping, where AM is used to decrease production time of prototypes. Another important application of additive manufacturing is in rapid tooling. Rapid tooling refers to use of AM to produce tools or tool parts similarly to decrease production time in comparison to conventional manufacturing of tooling. As AM is used with part 3D models, it requires use of STL file format to transfer the 3D model to the 3D printer. Operations performed on a 3D printed part after its AM process, whether a single or a multi-step process, in order to reach a desired final part is referred as post-processing. Principles of additive manufacturing process are depicted below in figure 1. (ISO/ASTM 52900:2015 2019.)

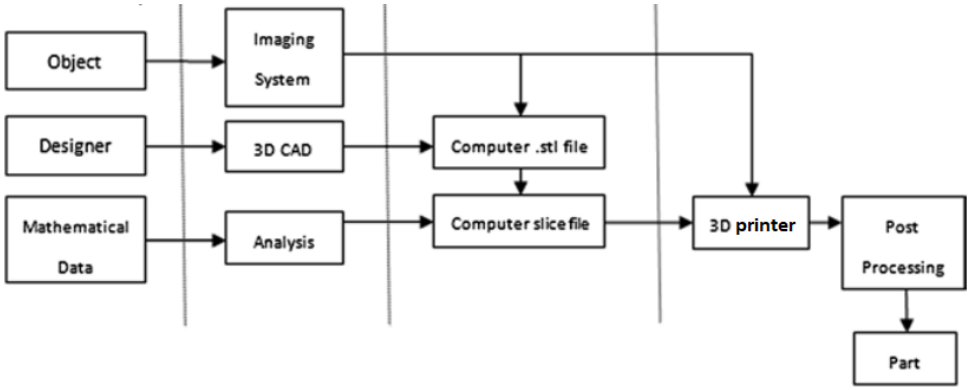

Figure 1. Principles of additive manufacturing process (Mod. Muthu and Savalani 2016, p. 3).

3D printing is a disruptive technology causing remarkable change in industries adopting it. In early stages of 3D printing technology adoption, it was used for rapid prototyping whereas nowadays due to advancement of the technology, industries can manufacture tools with 3D printing which are used for conventional manufacturing. It has thus become feasible to manufacture an end product completely with a 3D printer. Due to ongoing decrease in cost of 3D printing technology, its adoption is also increasingly accessible for SMEs (small and medium-sized enterprises) instead of being restricted to heavy industry. (Rayna and Striukova 2016, p. 214-217.)

The early stages of 3D printing technology trace back to 1980s back when its use was limited to plastic filaments. Likewise, in 1980s 3D printing itself was more time consuming, costlier and feasible only with smaller 3D printed objects resulting in lower print quality. In 1990s 3D printing technology had advanced to include use of metal alloys with 3D printers, enabling manufacturing of tooling with them. In 2000s the advancement of 3D printing technology had enabled high quality prints with low costs, facilitating manufacturing of end products. Today it is possible to manufacture an end product with a 3D printer entirely digitally, using only a CAD (Computer-aided design) model together with the 3D printer. Emergence of 3D printing technology adoption is best summarized in figure 2 below. (Rayna and Striukova 2016, p. 217.)

Adoption stage	Started	Design	Tooling	Manufacturing	Distribution
Rapid prototyping	Early 1990s	✓			
Rapid tooling	Late 1990s	✓	✓		
Direct manufacturing	Late 2000s	✓	✓	✓	
Home fabrication	Early 2010s	✓	✓	✓	✓

Figure 2. Different stages in 3D printing technology adoption (Mod. Rayna and Striukova 2016, p. 217).

Current manufacturing challenges in additive manufacturing has to do with ability to produce speedy part fabrication whilst providing dimensional control and guaranteeing a good surface finish of the part. Varying limits of quality control and part build volume between 3D printers are also adding up to difficulties with additive manufactured parts. Material consideration in AM brings about challenges of its own as material suitability for AM depends heavily on state of the material as well as on the used 3D printer and AM technique. State of the 3D printing material, also referred as feedstock, can be either powder, filament, sheet or even liquid. This in stark contrast with conventional manufacturing where feedstock consideration requires less focus as the material supplied is often pre-fabricated or pre-formed with standardized sizing and shaping. (Tofail et al. 2018, p. 24-26.)

Nowadays additive manufacturing can be used with metals. AM of metals involves use of a carefully chosen AM technique as metal as a feedstock requires special consideration in its binding mechanism during 3D printing. In metal 3D printing feedstock is metal powder or wire which is then melted layer by layer with help of a laser or electron beam depending upon used AM technique. The laser or electron beam must exceed melting temperature of the used metal as it is extruded on a build plate. Build plate must be pre-heated before 3D printing of metal to prevent thermal gradient of part and likewise during 3D printing some support structures need to be used to allow heat dissipation and to ensure the 3D printed metal part is fixed on the build plate. Preventing thermal gradients and allowing heat dissipation will ensure the 3D printed metal part will not deform during its 3D printing. Heating temperatures of 3D metal printers are considerably higher than that of other 3D printers. (Herzog et al. 2016, p. 371-372.)

1.5 Hybrid manufacturing

Benefiting both from advantages of additive manufacturing as well as conventional manufacturing requires their hybridization. Hybridization of AM technology with conventional, subtractive, technology such as computer numerical control (CNC) machining is referred as hybrid manufacturing. A machine which hybridizes AM and subtractive technology is referred as a hybrid machine. Hybridizing AM with CNC machining can cover for deficiencies typical to AM like dimensional accuracy and part surface finish. Finishing of 3D printed metal part is possible without process interruption as the very same hybrid machine can provide it thanks to this hybridization of AM and CNC machining. Principle of AM and CNC machining hybridization is depicted below in figure 3. (Yamazaki 2016, p. 82.)

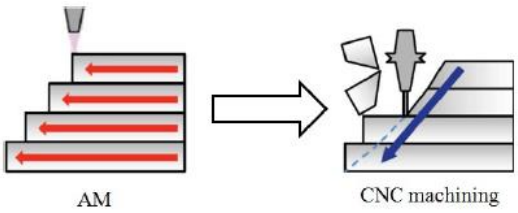

Figure 3. AM and CNC machining hybridization (Yamazaki 2016, p. 82).

Distinct advantages to hybrid manufacturing with AM and CNC machining method such as milling are ability to produce geometries allowing for internal cooling channels and hollow sections. Previous research also indicates of higher fatigue strength in hybrid manufactured parts than in AM parts due to better part surface finish. Hybrid manufacturing has been recognized economical with scarce metals due to reduced chip generation, and with materials difficult to machine due to reduced tool wear. Therefore, use of hybrid manufacturing is especially useful with high value products in which material costs are sizable. Resulting dimensional errors during AM steps in part hybrid manufacturing process can be fixed with alternating milling steps in between. Figure of a hybrid manufacturing process steps with AM and CNC milling is depicted next in figure 4. (Du et al. 2016 p. 2-3; Yamazaki 2016, p. 84.)

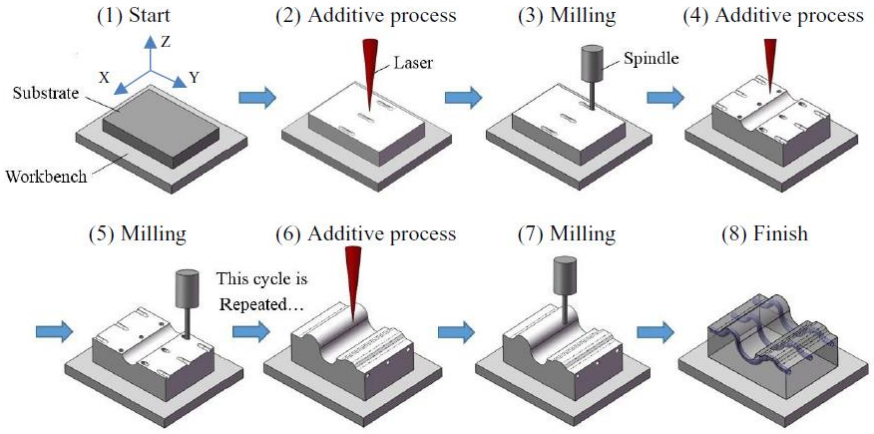

Figure 4. Hybrid manufacturing with AM and CNC milling (Du et al. 2016, p. 3).

Hybrid manufacturing machines are often limited to practical issues deriving from incorporation of AM and conventional manufacturing technology in mechanical design of a hybrid machine. Combining equipment necessary for both AM and conventional manufacturing method into one hybrid machine risks a result of complex mechanism. Preventing misalignment of equipment due to switch between AM and conventional manufacturing during a hybrid manufacturing process requires features such as sensors in a hybrid machine. Configuring hybrid machine axes requires special consideration for allowing axes movement and setting up the machine platform for vastly different manufacturing techniques adds up to complexity of hybrid machine control system. As AM involves high operating temperature as is the case especially with AM of metals, hybrid machine needs more measures for temperature control. (Amanullah et al. 2017, p. 165-169.)

1.6 Thread cutting tool

The studied part which is to be additive manufactured is a thread cutting tool. According to ISO 13399-1:2006 (2019) cutting tool is a "device or assembly of items for removing material from a workpiece through a shearing action at the defined cutting edge or edges of the device-- A cutting tool could be the assembly of one or more adaptive items, a tool item and several cutting items on a tool item.". The cutting tool performs cutting on a part which is referred as a workpiece whereas cut material from the workpiece done by this cutting is called a chip. The studied thread cutting tool consists of both a tool item and cutting item in its assembly. An illustrative figure depicting assembly of cutting tool is presented on next page in figure 5. (ISO/TS 13399-50:2013 2019.)

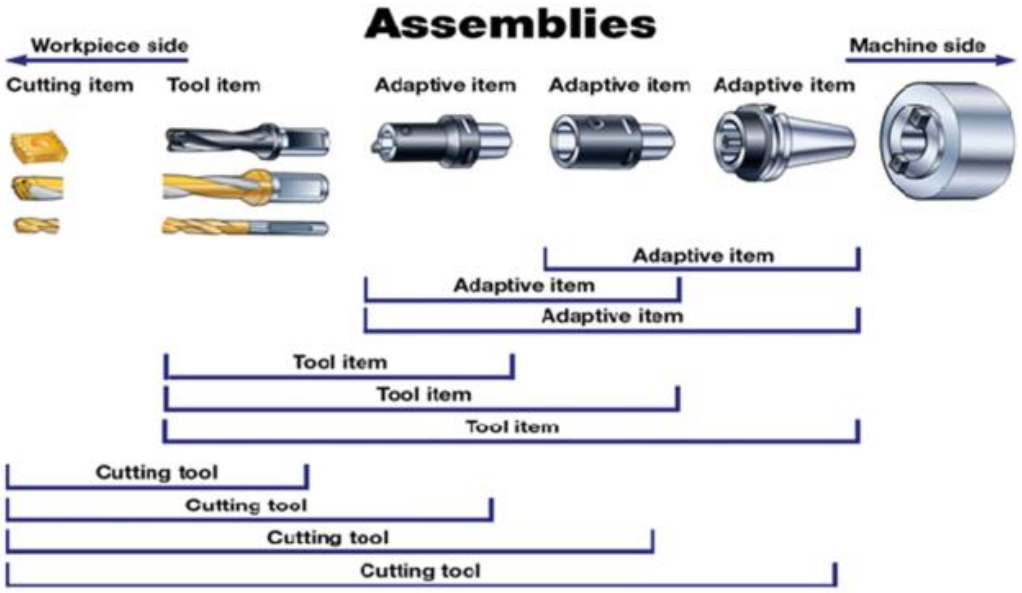

Figure 5. Possible assemblies of components of a cutting tool (ISO/TS 13399-50:2013 2019).

Thread cutting tool is a cutting tool used in manufacturing of external diameter threads. A screw thread, synonymous to thread in context of this study, refers to a ridge shape on inter or outer surface of a cylinder with form of the ridge depending upon type of the thread. Common types of threads are straight threads where the ridge is in form of helix, and tapered threads where the ridge is in form of conical spiral. Application of tapered threads is mostly with pipe joints whereas straight threads are widely spread in fasteners. Important nomenclature in screw threads are pitch and lead as well as major, minor and pitch diameter. (Black and Kohser 2012, p. 1181-1182.)

Prevalent screw thread standard systems are Unified and American Screw Thread Standards or Unified system as commonly known, and a set of metric standards from International Organization for Standardization (ISO) which are commonly referred as ISO or metric system. In metric system pitch is expressed in millimeters whereas in Unified system it is expressed in amount of threads per inch. Explanations about the important nomenclature in screw thread is depicted next in figure 6. (Black and Kohser 2012, p. 1181-1182.)

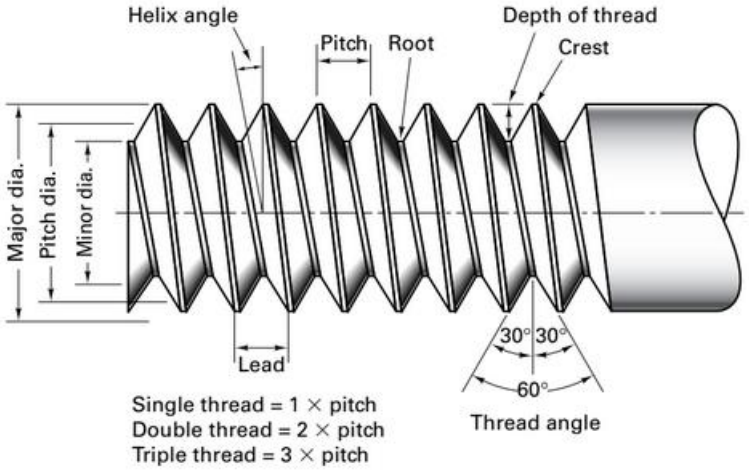

Figure 6. Nomenclature in screw thread (Mod. Black and Kohser 2012, p. 1182).

A great many types and series of screw threads can be considered with equivalent series both in the metric and Unified system. Thread profile differs on internal and external thread as well as in different thread series of the thread standard systems. Crest in external thread is either flat or rounded whereas root is only rounded to reduce concentration of stress. Crest in internal thread is flat for mating it with external thread and root is rounded for clearance. Type or series of the screw thread is displayed in its designation both in the metric and Unified system. The designation of a thread type depicts information regarding its thread specification as well as other parameters about it depending upon the thread standard system. Exemplary designations both in metric and Unified systems are provided next in figures 7 and 8. (Black and Kohser 2012, p. 1182-1185.)

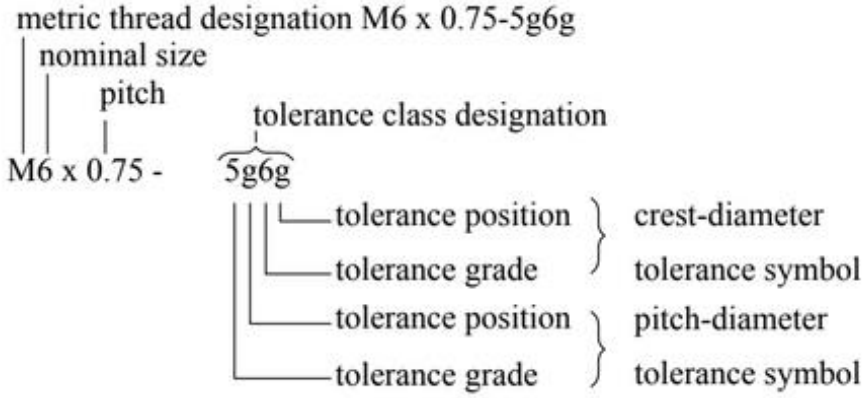

Figure 7. Thread designation in metric system (Mod. Black and Kohser 2012, p. 1185).

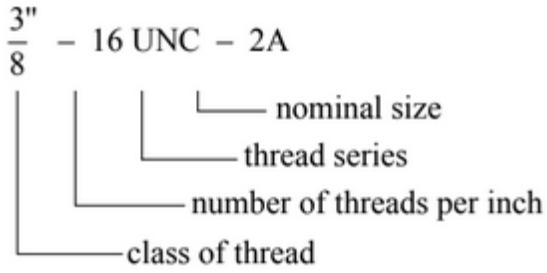

Figure 8. Thread designation in Unified system (Mod. Black and Kohser 2012, p. 1185).

1.7 Tapping

A process in which an internal thread is made into a drilled hole by cutting with the use of a multiple point cutting tool is referred as thread tapping, or merely as just tapping. The multiple point cutting tool used in tapping is referred as tap. Tapping motion is rotary and direction of tapping is vertical perpendicularly to tap's axis of rotation. The drilled hole in which the internal thread is to be tapped should have a diameter which is slightly larger in comparison with the minor diameter of the thread. Type of a tap depends on its nomenclature, namely its flute and whether the end of the tap is tapered or straight. Flutes divide cutting edges on profile of the thread whilst allowing space for chips and cutting fluid. Cutting fluid can be a coolant or a lubricant, with purpose of decreasing heat or friction generated during tapping. Taps are commonly made of either high-speed steel or carbon steel and often coated with titanium nitride (TiN). Nomenclature of a tap is depicted next in figure 9. (Black and Kohser 2012, p. 1190; DORMER 2013, p. 23.)

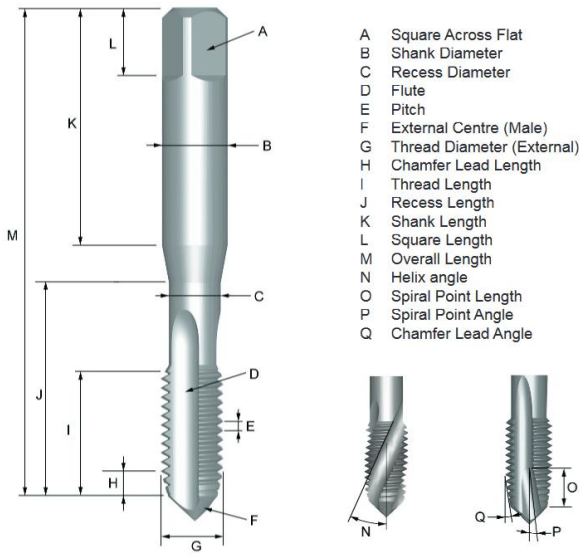

Figure 9. Nomenclature of a tap (Mod. DORMER 2013, p. 64).

As mentioned, there are different types of taps with varying shapes of flute with tapered or straight tap ends. Straight fluted taps are typically used with materials producing short chips whereas spiral fluted taps are used with materials producing long or spiral chips. Spiral point taps are used with through holes as the shallow-shaped flute pushes chips forward. Tapered tap, as the name indicates, has a tapered end with gradually increasing thread depth to facilitate tap alignment and to decrease tap torque. To tap a blind hole a set of 3 taps are used consecutively; taper tap, plug tap and bottom tap. Taper tap aligns the thread of the hole whilst plug tap provides full thread depth and bottoming tap finishes remaining threads at the very bottom of the threaded hole. Some of the types of taps are depicted next in figure 10. (Black and Kohser 2012, p. 1190; DORMER 2013, p. 66-67.)

Figure 10. Different types of taps (Mod. DORMER 2013, p. 66-67).

1.8 Additive manufactured cutting tools

Due to relatively late emergence and advancement of AM techniques in producing metallic end products, there are only limited instances of AM application in literature and industry especially in the field of cutting tools. One significant driver for AM adoption has been recognized as improved ability to design a cutting tool with internal cooling. Improving internal cooling of a cutting tool namely reduces its cutting temperature and prolongs its tool life. Excessive heat generated during use of a cutting tool affects both tool wear and workpiece surface quality. However, an internally cooled cutting tool contains complex cooling channels which makes its manufacturing impossible using merely conventional manufacturing. (Ghani et al. 2017, p. 2.)

Complex cooling channel of a cutting tool consist of an inlet and outlet which allow for a flow of a cutting fluid typically through tip of a cutting tool if not through its shank in addition. Flow of cutting fluid through the cooling channel can be severely affected by defects in the channel geometry, requiring careful consideration for dimensional accuracy as it is one of the disadvantages of many AM techniques. Example of a cutting tool design with internal cooling channels which is to be 3D printed is seen next in figure 11. (Ghani et al. 2017, p. 2-3.)

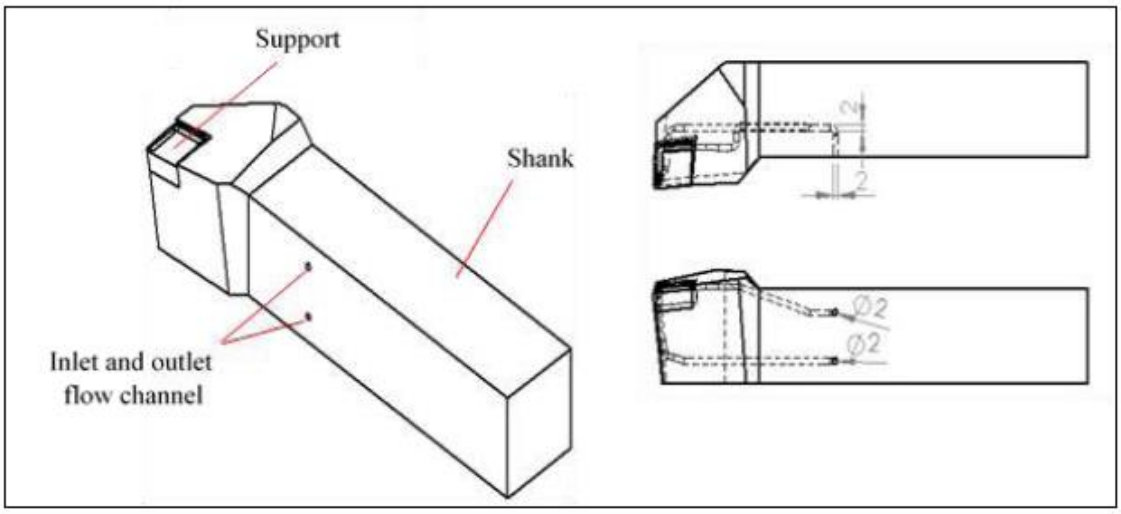

Figure 11. Internally cooled cutting tool design for 3D printing (Mod. Ghani et al. 2017, p. 3).

Due to insufficient properties of metals for application areas such as corrosive environments, AM of ceramics provides an effective alternative even for cutting tools. AM technique used with ceramic material can be done directly without post-processing or indirectly with post-processing. 3D printing a ceramic cutting tool without post-processing likely results in defects due to residual stresses and poor surface roughness. 3D printing the cutting tool in preparation for post-processing involves use of a binder material together with the ceramic feedstock. The use of binder material enables post-processing methods such a debinding and drying of the additive manufactured ceramic cutting tool both of which are necessary for their successful manufacturing with AM. Ceramic cutting tools such as those made of alumina provide desirable mechanical properties in addition to advantageous chemical resistance for their use in a corrosive application area. (Zhou et al. 2016, p. 11598-11599.)

Debinding and drying of additive manufactured alumina cutting tool can enable production of alumina cutting tool with dense microstructure whilst eliminating formation of cracks and pores. Large pores cannot form into the additive manufactured cutting tool as water is evaporated from the AM sample by drying. Defects or cracks resulting from pressure caused by high temperature of post-processing processes are prevented by debinding with use of vacuum for air debinding before binder material removal. Figure 12 below shows 3D printed alumina cutting tool cutting item without major defects. (Zhou et al. 2016, p. 11599-11601.)

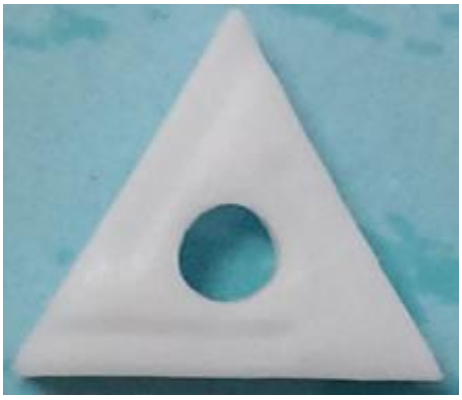

Figure 12. 3D printed alumina cutting tool cutting item without major defects (Mod. Zhou et al. 2016, p. 11602).

Another significant driver for AM adoption with cutting tools has been design optimization, as discussed previously. Manufacturing a cutting tool from an expensive cutting tool material such as cemented tungsten carbide requires a minimized material use for its manufacturing which can be offered by AM. AM provides an alternative for manufacturing a cemented tungsten carbide tool with an optimized design allowing its weight reduction whilst upholding its performance and quality necessary for the cutting tool usage. By reducing weight of the cutting tool, manufacturing time and costs are also reduced. Moreover, a cutting tool with a reduced weight enables more accurate high-speed operations as machinery using the cutting tool can then move the tool faster along its tool path. (Stoyanov 2016.)

AM produced cutting tool with optimized design allowing its weight reduction can have internal cavity. The internal cavity on the other hand consist of supports and interior surface. The supports, interior surface and cavity form interior of the optimized cutting tool design whereas exterior is formed by the exterior surface. One optimally designed cutting tool consisting of this described geometry which is enabled by AM is shown next in figure 13. (Stoyanov 2016.)

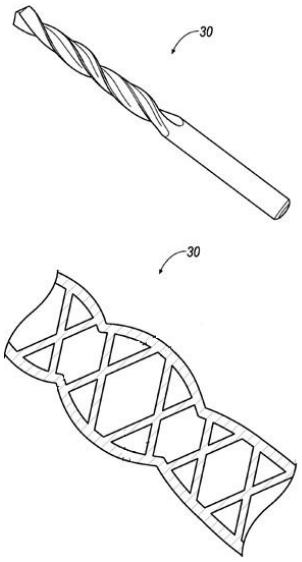

Figure 13. 3D printed cutting tool with optimized design enabling weight reduction (Mod. Stoyanov 2016).

1.9 Finite element method (FEM) tapping simulation

Use of numerical methods like finite element method is common in metal cutting studies such as those about tapping or taps. FEM or alternatively finite element analysis (FEA) is often applied in metal cutting simulation, with aim of predicting different outputs and characteristics like cutting forces or stresses of the cutting process. These FEA simulations therefore can offer valuable information about stress distribution and deformations. Validity of FEA results depend heavily on boundary conditions of simulated model about the metal cutting process. Boundary conditions rest on assumptions and simplifications which should be represented accordingly about the studied metal cutting process. (Astakhov and Outeiro 2008, p. 13.)

FEM simulations about tapping have been recognized as limited in the literature by Oezkaya and Biermann (2017) due to difficulty in simulating tapping torque (*M*) throughout tap chamfer length as it would require undesirably lengthy computing time. Oezkaya and Biermann (2017) likewise worked out to decrease 3D FEM tapping simulation computing time by constructing segmented and mathematical model for tapping torque prediction. Workpiece in a reference model with torque values derived from experimental testing was disassembled into volume segments for computing time reduction and the segmented model was then evaluated before mathematical model was developed for calculating highest tapping torque values in the segmented model. The constructed segmented and mathematical model successfully reduced computing time of 3D FEM tapping simulation for tapping torque prediction, as seen next in figure 14, whilst still leaving out other boundary conditions such as surface roughness as well as coolant and lubricant influence. (Oezkaya and Biermann 2017, p. 707.)

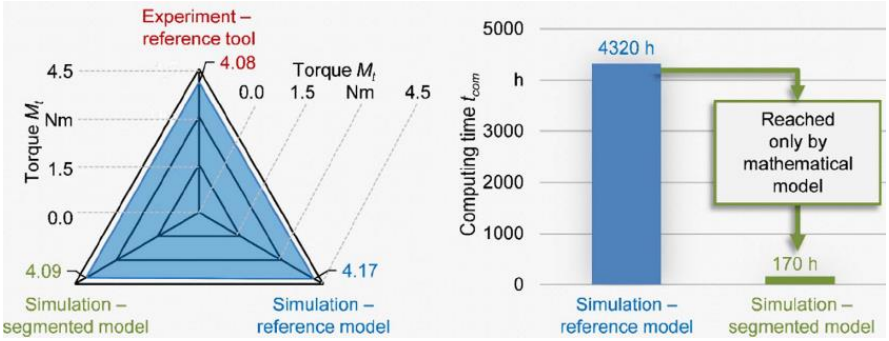

Figure 14. Tapping torque prediction and computing time of 3D FEM tapping simulation models (Mod. Oezkaya and Biermann 2017, p. 707).

Peng et al. (2016) studied tapping performance by altering different tap parameters like hook rake and relief angles, explained consequently in figure 15, in their 3D FEM tapping simulation about HSS M8 x 1.25 tap in orthogonal test. Regression analysis between cutting force components and the different tap parameters as seen in figure 16 and 17 next indicated of tap rake angle increase as resulting in reduction of the cutting forces with Ti-6Al-4V alloy workpiece. Increasing tap relief angle on the other hand reduced axial and radial forces (F_z and F_y) but increased circumferential force (F_x). Consequently, rake angle was determined to have a bigger influence on tapping performance than relief angle. (Peng et al. 2016, p. 1114-1120.)

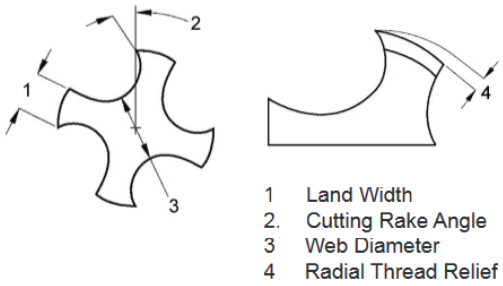

Figure 15. Tap nomenclature, showcasing rake, and relief angle (Mod. DORMER 2013, p. 64).

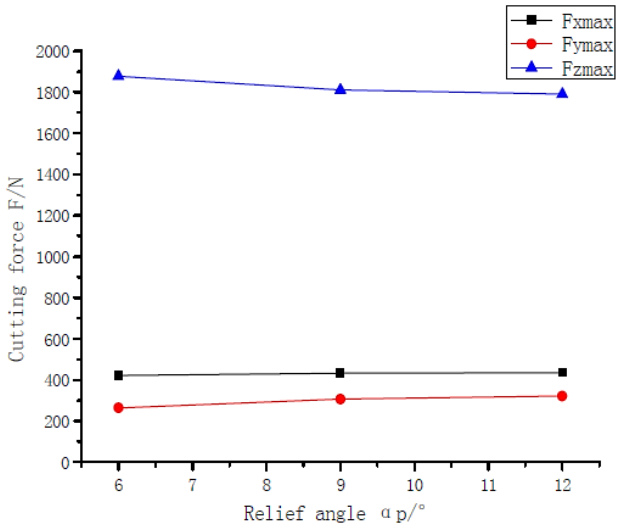

Figure 16. Relief angle regression analysis on cutting force components (Mod. Peng et al. 2016, p. 1118).

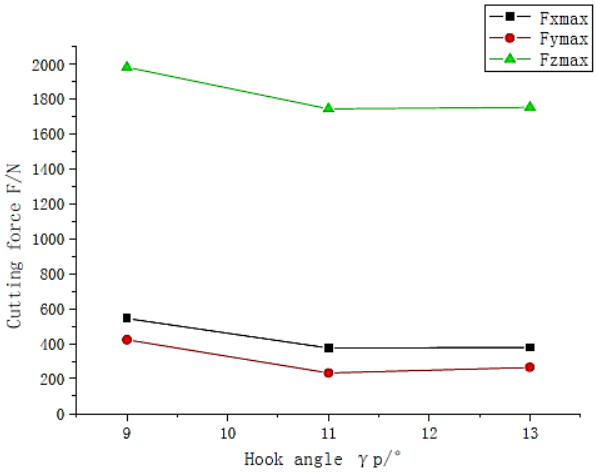

Figure 17. Hook rake angle regression analysis on cutting force components (Mod. Peng et al. 2016, p. 1118).

Influence of tap hook rake angle and flute angle on chip curling in tapping was observed by Tang et al. (2011) on TC4 titanium alloy workpiece. Chip curling was simulated with 3D FEM model before comparing the simulation results with data from tapping tests using both a standard tap and modified-tooth taps with separate flute forms and rake angles. FEM results depicted a smaller tap rake angle making chip curling more effective, thereby enhancing chip removal. (Tang et al. 2011, p. 1286-1290.)

Tapping test data showed modified-tooth tap as having smaller tapping torque than the standard tap. The modified-tooth tap with standard flute was concluded as being more effective in chip removal than the modified-tooth tap with 85° flute in continuous tapping with increasing cutting speed (v_c) due to its downward trending tapping torque, as highlighted below in figure 18. (Tang et al. 2011, p. 1286-1290.)

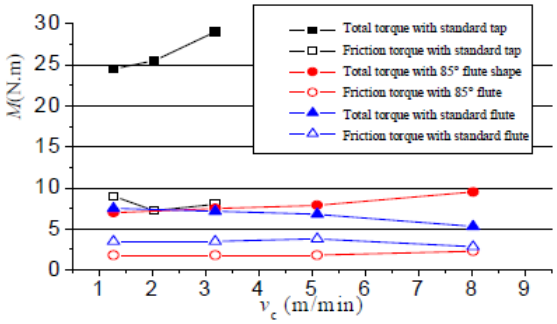

Figure 18. Tapping torque comparison between a standard tap and modified tooth-taps in continuous tapping with increasing cutting speed (Tang et al. 2011, p. 1290).

2 DESIGN AND TOPOLOGY OPTIMIZATION

Procedure for design and topology optimization of M16 thread tap is laid out in this chapter. Utilized 3D FEM tapping model in the thesis work is firstly presented before a step by step process of M16 tap design optimization through altering of tap parameters. The tap design optimization is followed by topology optimization, with different tap crown topology configurations being compared among themselves in order to choose most suitable ones for their 3D printing. The topology configurations are showcased whilst given topology requirements are derived. Preparation of the chosen tap crown topology configurations for 3D printing is discussed, and finally 3D printing results of the optimized tap crown samples are revealed to determine their suitability for their post-processing as well as experimental tapping tests.

2.1 Standard M16 tap design with simplified FEM simulation

M16 x 2 HSS T15 tap is designed according to Thurmer's technical drawing utilizing SolidWorks CAD-software. Technical drawing of M16 tap is displayed in Appendix 1. After designing the tap, a static study is created in SolidWorks where tapping torque is set to be applied on the tap shank and cutting edges of the tap are fixed. This static study setup will comprise the simplified FEM tapping simulation used in design and topology optimization of M16 tap. Meshing for the simulation is as fine as standard mesh of SolidWorks allows, and utilized T15 material data values together with chemical composition are displayed next in table 1 and 2.

Table 1. T15 specifications

Density	8.19 g/cm^3
Tensile strength at 20 °C	1630 MPa
Yield strength at 20 °C	1250 MPa
Powder particle size	15-53 µm

Table 2. T15 chemical composition

Element	T15 (wt%)
Tungsten, W	11.75-13.00
Cobalt, Co	4.75-5.25
Vanadium, V	4.50-5.25
Chromium, Cr	3.75-5.00
Carbon, C	1.40-1.60
Manganese, Mn	0.15-0.40
Silicon, Si	0.15-0.40
Phosphorus, P	0.03 max
Sulfur, S	0.03 max
Iron, Fe	Balance

Value of tapping torque for M16 tap is derived from an industrial catalogue of Fanar, another cutting tools manufacturer, and as such the utilized tapping torque value is a recommended torque value for M16 tap when tapping workpiece material with tensile strength of 1000 MPa. As tapping torque causes a high concentration of stress on the cutting edges of the tap, more reflective values of stress distribution should be measured from the tap crown geometry below the cutting edges. Hence the tap crown is split into 3 cross sections, and maximum stress values will be measured from each of these tap crown cross section to provide more reflective stress values. Cross sections are 86, 95 and 103 mm from tap shank square into the tap crown, dividing the tap crown in roughly 3 sections below the cutting edges. Recommended tapping torque values from Fanar, and static study setup of the simplified FEM tapping simulation can be seen below in figures 19 and 20.

Thread M	Torque [Nm]
3	0,5
4	1,2
5	2
6	4
8	8
10	16
12	22
14	36
16	40
18	63
20	70
22	80
24	125
27	140
30	220
33	240

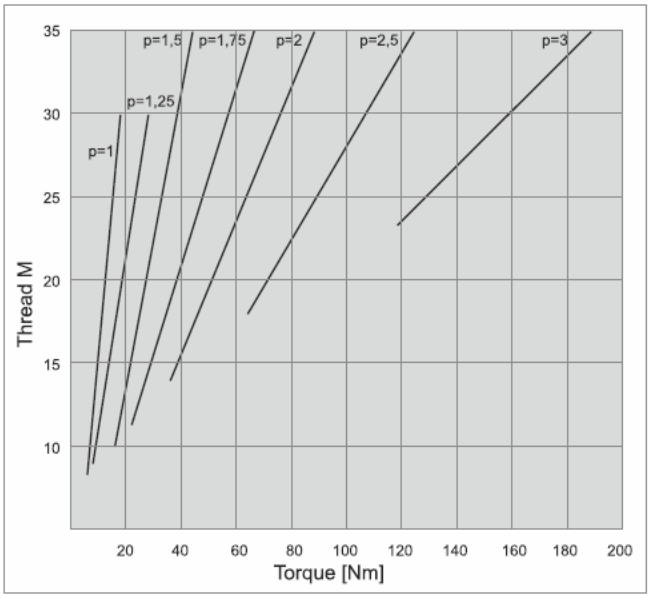

Figure 19. Tapping torque values with 40 Nm for M16 tap (Mod. Fanar 2018, p. 256).

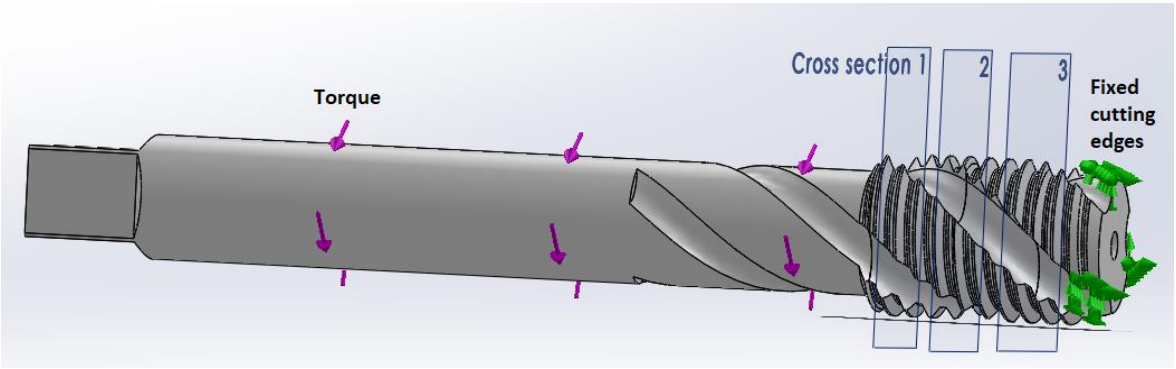

Figure 20. Simplified FEM tapping simulation setup

2.2 Flute geometry

First M16 tap parameters to optimize are those on its flute geometry; flute (lead) angle and rake angle. Design optimization starts with flute angle through parametric optimization by running design studies in SolidWorks. Flute lead angle is defined as "Angle at which a helical or spiral cutting edge at a given point makes with an axial plane through the same point." (Oberg et al. 2000, p. 874). The studied standard M16 tap design consists of 3 spiral flutes as is seen from figure 20 and Appendix 1. Flute angle is determined from flute helix diameter and lead, the helix lead being also referred as helix pitch. Flute lead angle is illustrated below in figure 21.

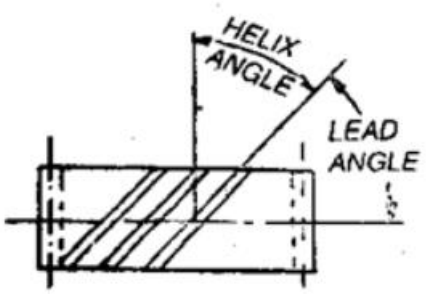

Figure 21. Representation of flute lead angle (What-when-how, 2019).

As mentioned, flute lead angle consists of helix diameter and pitch. Helix diameter is same as with the tap thread diameter and constant, 16 mm, whereas pitch is taken from technical drawing of the standard M16 tap design. Flute angle can be calculated as follows (equation 1).

$$\arctan \lambda = \frac{L}{\pi * D} \quad (1)$$

In equation 1 above λ is flute lead angle, L is helix pitch and D is helix diameter (Mod. Radzevich 2012). Helix pitch is chosen as a variable for design study in SolidWorks. The design study automatically runs the static study setup described above while helix pitch is increased and decreased to observe how stress distribution is affected by altering flute lead angle of the tap. Figure 22 on next page depicts results for stress distribution on the 3 different tap cross sections, stress 1 being the cross section on tap crown closest to the tap shank and stress 3 is the cross section closest to the tap cutting edges.

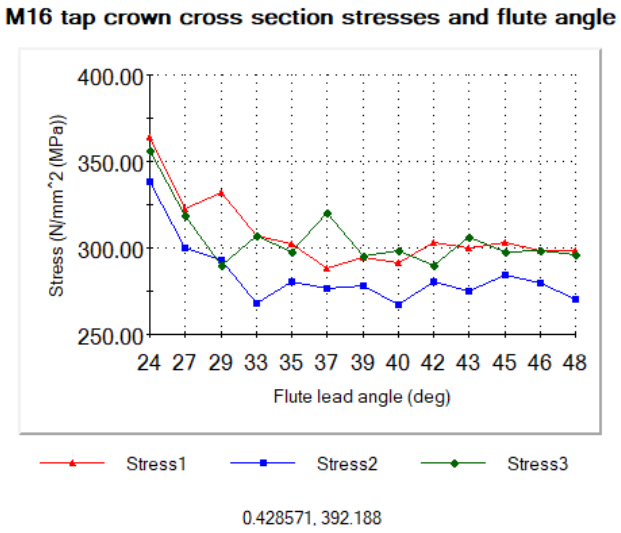

Figure 22. Design study results for optimal flute lead angle

After optimal flute angle, 40 degrees, is selected for the tap, a similar design study is run to derive optimal rake angle for the tap by increasing and decreasing rake angle as a design study variable while measuring its effect on tap crown cross section stresses. Optimal flute angle is used in the tap design while running design studies for rake angle. Rake angle has been illustrated and described previously in figure 15. Rake angle is limited to 7-13 degrees to allow multifunctional use of the tap with many workpiece materials according Fanar's industrial catalogue (Fanar 2018, p. 239). Figure 23 below depicts derived optimal rake angle as 12 degrees in the design study.

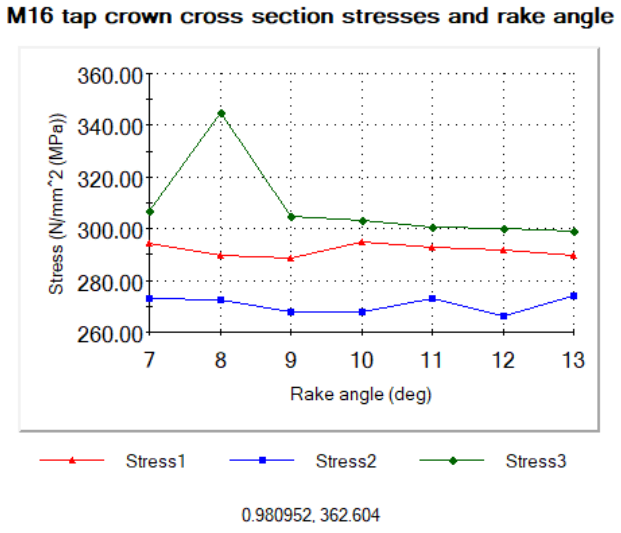

Figure 23. Design study results for optimal rake angle

2.3 Chamfer

Chamfer of a tap is defined as “Tapering of the threads at the front end of each land or chaser of a tap by cut-ting away and relieving the crest of the first few teeth to distribute the cutting action overseveral teeth.” and chamfer angle moreover as “Angle formed between the chamfer and the axis of the tap measured in an axial plane at the cutting edge.” (Oberg et al. 2000, p. 863). Chamfer form in the studied M16 tap is form C, which gives chamfer length tolerance as 2-3 threads and chamfer angle tolerance as 17-20 degrees according Thurmer’s technical drawing as seen in Appendix 1. Tap chamfer illustration is shown below in figure 24.

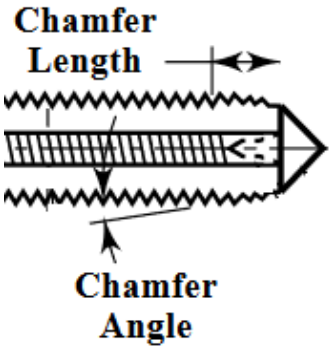

Figure 24. Representation of tap chamfer (Mod. Oberg et al. p. 863).

A similar procedure is carried out for deriving optimal chamfer angle and chamfer length of the tap as with optimizing flute geometry. Design studies are compiled firstly for choosing chamfer angle by using previously selected optimal values for flute angle and rake angle. Lastly a design study is run for finding optimal chamfer length by using optimal values for flute angle, rake angle and chamfer angle. Results from design studies of chamfer angle and chamfer length are revealed in Appendices 2 and 3. Derived optimal values are 17 degrees for chamfer angle and 2 threads for chamfer length. Pitch of M16 tap is 2 mm with 2 threads standing for 4 mm consequently.

2.4 Comparison of internal structures

After design optimization of the tap by selecting optimal values for flute angle, rake angle, chamfer angle and chamfer length the tap is lastly topology optimized. The design optimization enhances tap crown material reduction in the topology optimization as the optimal abovementioned tap parameters have been chosen to minimize stress distribution along the tap crown, thereby making the tap design stronger and increasing tap crown material removal potential. Topology optimization is done with use of internal square, pentagon, hexagon and circle grid structures as well as with internal hollow structure. The internal structures are aligned spirally with the tap flute helix to prevent their disorderly interference with the tap exterior and to preserve uniform margins with the tap exterior. The designed internal structures are visualized below in figure 25.

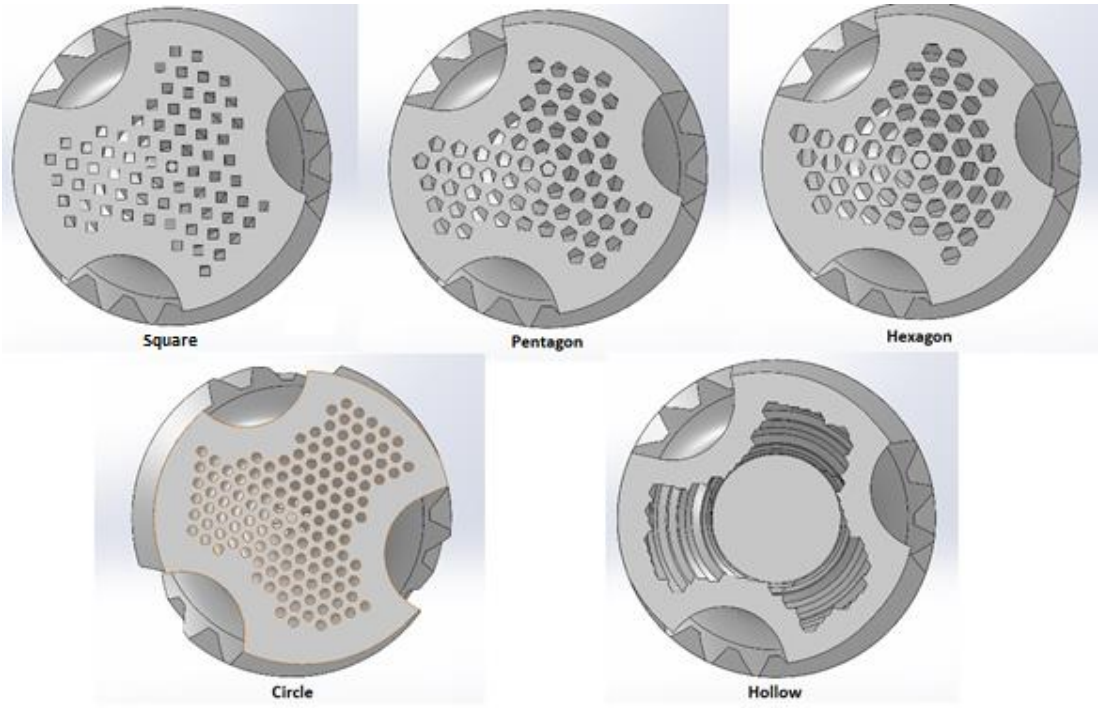

Figure 25. Different internal structures used in topology optimization

Minimum size and spacing for the internal grid structures are restricted by 3D printability. Minimum size must be 0.5 mm and spacing 0.3 mm as shown in figure 26 due to print layer height used by Thurmer's R&D project partner responsible with 3D printing of the tap crowns. Minimum margins have been found to be 1.2 mm to avoid interference with tap exterior and to avoid excessive stress distribution while designing the internal structures and running static studies with the used numerical tapping simulation model. Safety value for stress distribution below cutting edges is chosen as 800 MPa with the aim of having smaller stress values than that on the tap crown cross sections when tapping simulating the tap crown with the different internal structures. Initial internal structures lack several additional restrictions imposed on optimized internal structures, which are described hereafter and seen below in figure 27.

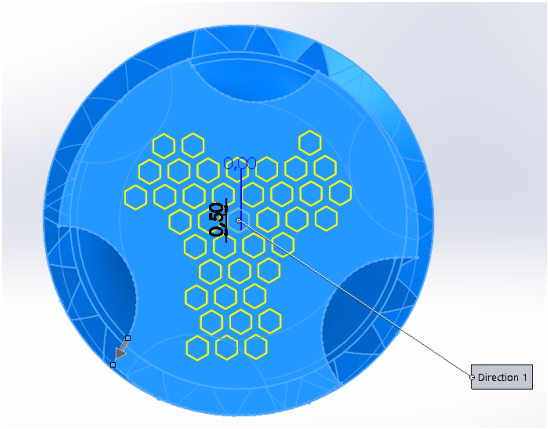

Figure 26. Minimum sizing and spacing in internal grid structures

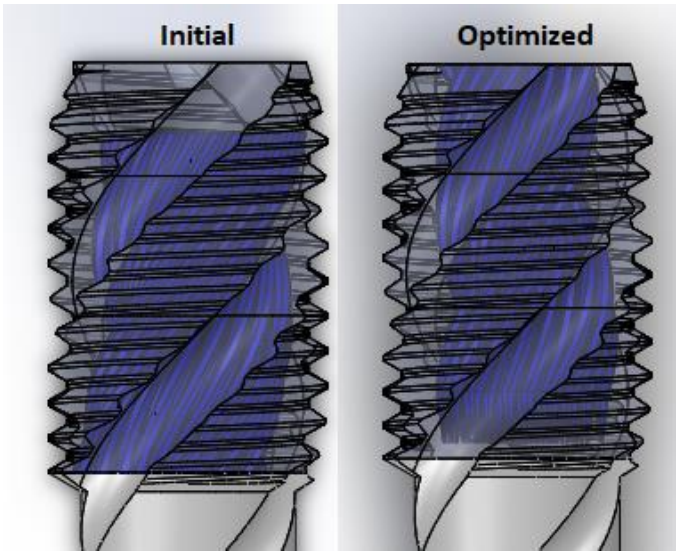

Figure 27. Initial and optimized hexagonal internal grid structure compared in blue

Optimized internal structures have a 3 mm long thickness transition on their bottom before their full and spiral geometry along the tap crown to avoid tap crown breakage in the tapping tests due to excessive stress distribution on sharp internal geometrical changes in the tap crown. Optimized internal structures contain a 3 mm gap from bottom face of the tap crown to allow its friction welding with conventionally manufactured shanks as per requirements from Thurmer's R&D project partner responsible with friction welding of the tap crowns and shanks. Thickness transition and gap between joint of tap crown and shank with internal structures are seen next in figures 28 and 29.

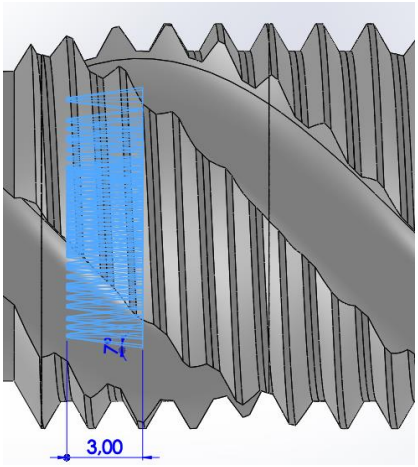

Figure 28. Thickness transition on bottom of an optimized internal structure

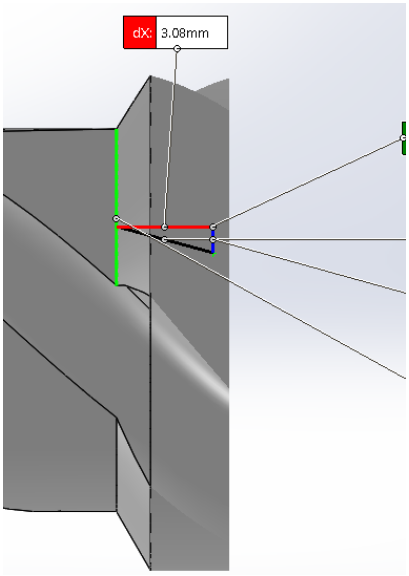

Figure 29. Gap between internal structures and joint section of tap crown with shank

Optimized internal grid structures cut through top face of the tap crown to enable release holes for metal powder inside the internal structures. In case of the optimized internal hollow structure, a release hole is designed to cut through the cone on the tap crown top face. Release holes in case of optimized internal grid structure and hollow structure are depicted below in figure 30. Lastly, optimized internal structures contain a widened margin of 1.5 mm with the tap crown exterior to further decrease stress distribution and to decrease likelihood of tap crown breakage during the tapping tests thanks to increased wall thickness. Tap crown exterior margin with optimized internal structure is shown in figure 31.

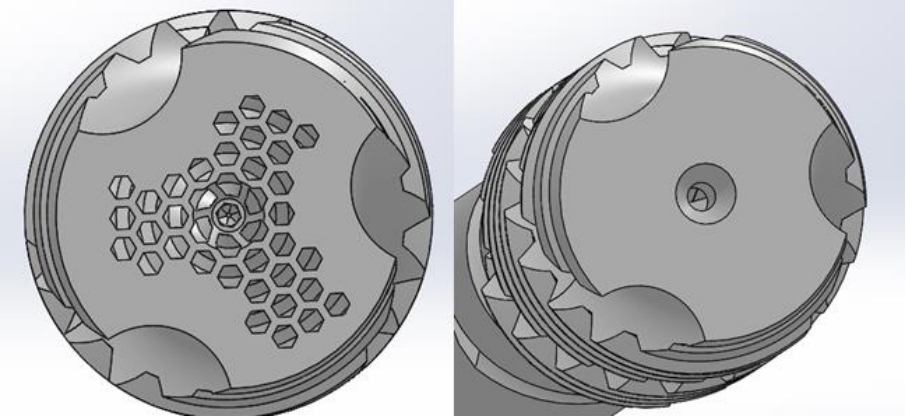

Figure 30. Metal powder release holes in optimized tap crown topology configurations

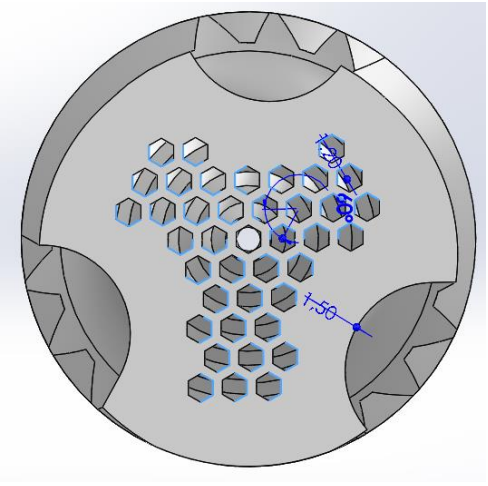

Figure 31. Tap crown exterior margin with optimized hexagon topology configuration

Initial internal structures lack these additional restrictions and as a result depict larger tap crown mass reduction capability with larger measured maximal stress values on the tap crown cross sections as can be observed in topology optimization results of Appendix 4. Circle internal grid structures lack maximum tap crown cross section stress values due to mesh failures and are not depicted in the Appendix 4 consequently. Initial and optimized circle topology configurations result in 16 % and 13 % tap crown mass reduction respectively.

2.5 Optimized designs for 3D printing and testing

Out of all tap configurations compared in the topology optimization, 3 designs are chosen for 3D printing and experimental tapping tests. Design optimized M16 tap crown is chosen for 3D printing and testing to obtain reference values of tapping torque and to validate effect of altering the tap parameters in comparison to the standard M16 tap design. Optimized hexagon and hollow internal structures are chosen for 3D printing and testing from the different tap crown configurations studied in the topology optimization. Optimized hollow and hexagon configurations are chosen due to them allowing largest tap crown mass reduction while also not exceeding the safety value of 800 MPa on the tap crown cross sections as observed in Appendix 4. Sketch filleting is done for both hexagon and hollow internal structures to reduce sharp edges in the internal geometries of the 3D printed tap crowns as a precaution for reducing the risk of tap crown breakage in the tapping tests.

Preparation of the chosen optimized designs for 3D printing is continued by suppressing thread and chamfer of the tap crown and expanding the tap crown diameter by an oversize of 0.3 mm. Oversize is used to compensate for material shrinkage occurring during 3D printing of the tap crowns, and for grinding done on the 3D printed tap crown samples afterwards to reduce their surface roughness in addition to grinding their external thread geometry. Prepared optimized design for 3D printing containing oversize, suppressed thread and chamfer is depicted in figure 32 next.

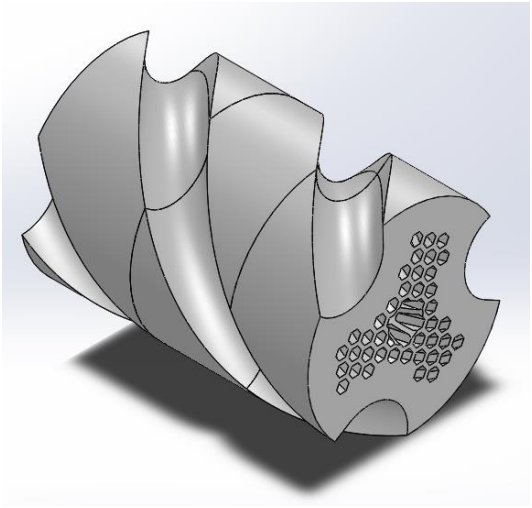

Figure 32. Tap crown design prepared for 3D printing

The M16 tap crown designs chosen for 3D printing are lastly converted from their 3D CAD models to STL files which are send to an additive manufacturing system used to 3D print the tap crown samples. Tapping torque value used in the numerical model will be compared with experimentally measured tapping torque from the tapping tests to validate accuracy of the simulated results. The chosen optimized tap configurations for 3D printing are displayed below in figures 33 and 34.

Figure 33. Optimized hexagon internal grid structure for 3D printing

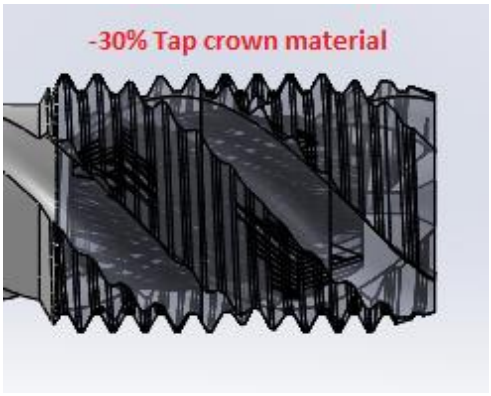

Figure 34. Optimized hollow internal structure for 3D printing

2.6 Additive manufacturing and post-processing of tap crowns

Chosen design optimized M16 tap crown as well as the optimized M16 tap crown designs with hexagon and hollow internal structures are 3D printed using selective laser melting (SLM) technique. Selective laser melting is to be done with Renishaw AM400 additive manufacturing system. 3 samples of design optimized tap crown are 3D printed whereas 2 samples of optimized hexagon and hollow topology configurations are 3D printed, bringing the total amount of 3D printed samples to 7. After 3D printing of each sample a visual inspection is done on the samples for observation of their porosity. The utilized Renishaw AM400 additive manufacturing system is seen in figure 35.

Figure 35. Renishaw AM400 used for 3D printing the optimized M16 tap crown designs (Renishaw 2015, p. 1).

In SLM the HSS T15 powder is spread on a pre-heated platform before it is fused selectively with a laser beam on a layer by layer basis finally forming the tap crown geometry. The laser beam is moved by a scanner and the platform moves automatically downward by the used layer height after melting of one layer. Layer height is limited by T15 powder particle size as previously shown in table 2 of T15 material specifications. This process repeats after each layer of the optimized tap crown sample has been melt by the laser beam, finally bringing the process to an end with the completion of the build tap crown sample. This process is visualized below in figure 36.

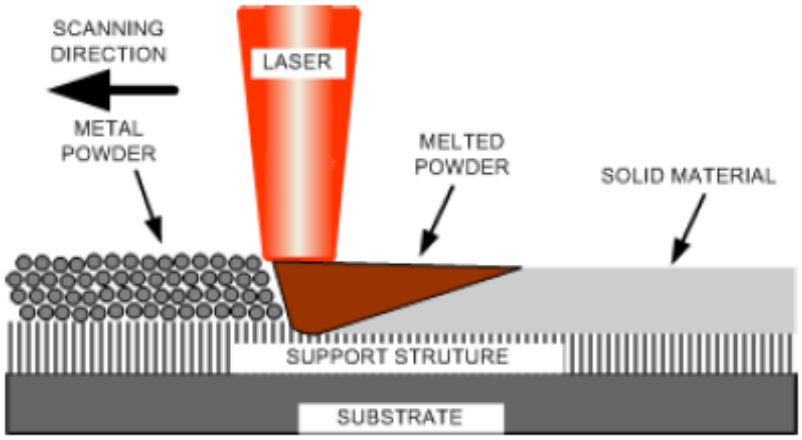

Figure 36. SLM process principles for 3D printing the tap crown samples (Mod. Kurzynowski et al. 2012, p. 2).

3D printed tap crown samples are to be joined with conventionally machined tap shanks by friction welding. Friction welding is a joining method in which two mechanically contacted surfaces are joined together via frictional heat generation and forging pressure. Friction welding process used to join the tap crown with the tap shank is inertia friction welding. In inertia friction welding the tap crown is stationary while the tap shank is attached to the crown through a rotating flywheel. After contact is made between the rotating tap shank and the stationary tap crown by applying pressure, the rotating tap shank generates frictional heat which then creates a weld. Inertia friction welding process is illustrated next in figure 37. (Yilbas and Sahin 2014, p. 1-2.)

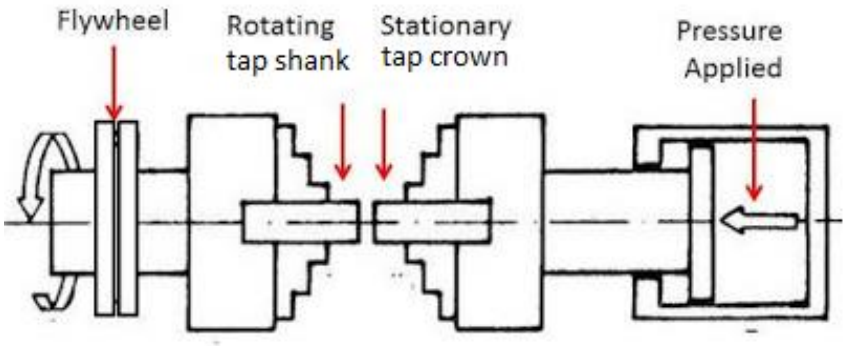

Figure 37. Principle for inertia friction welding tap crown with tap shank (Mod. Mech4study 2019).

Heat treatment of the brittle 3D printed tap crowns is required before their friction welding with the tap shanks. The 3D printed samples are to be quenched and tempered before friction welding, and after their friction welding with the tap shanks their post-processing is done by grinding. The friction welded hybrid taps are grinded to reduce their resultant surface roughness from 3D printing and to produce desirable tap thread, flute and chamfer geometries.

3D printing procedure for the optimized tap designs was started by a series of test prints with T15 samples. In test printing, several printing parameters were modified to allow for high consolidation in the test T15 samples. Adjusted printing parameters were laser power, scanning speed, hatch distance, laser exposure time and point distance. Build chamber platform was pre-heated as high as possible, 170 °C, given capabilities of Renishaw AM400. Test prints indicated of brittle fractures and lack of fusion in the T15 test samples, as can be noted in figure 38 below.

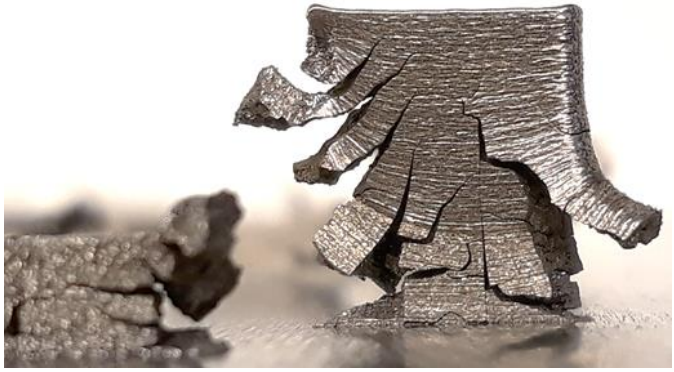

Figure 38. T15 test prints with brittle fractures and lack of fusion

Test print samples with least cracking were considered in selecting parameters for printing the tap crown samples. Tap crown cylinders were printed with flute geometry being suppressed in addition to the previously suppressed tap crown features in their preparation for 3D printing. Tap crowns were printed without flute geometry to advance consolidation of the prints due to heavy cracking noted in the test print samples. Altered 3D printing parameters with tap crown cylinders are displayed in table 3 and utilized 3D printing parameter configurations are shown afterwards in figure 39.

Table 3. T15 printing parameters

Laser power	100-200 W
Scanning speed	1600-3000 mm/s
Hatch distance	0.05-0.09 mm
Laser exposure time	40 µs
Point distance	80-150 µm

Point distance	Hatch distance	Exposure time	Scanning speed	2D energy density	Laser power
115	0.07	40	2300	0.75	150
115	0.09	40	2300	0.58	150
150	0.07	40	3000	0.57	150
150	0.05	40	3000	0.53	100
80	0.05	40	1600	2.00	200
115	0.05	40	2300	1.04	150
80	0.07	40	1600	1.07	150
115	0.07	40	2300	0.75	150
115	0.07	40	2300	0.75	150
150	0.09	40	3000	0.30	100
115	0.07	40	2300	0.50	100
115	0.07	40	2300	0.75	150
80	0.05	40	1600	1.00	100
115	0.07	40	2300	0.75	150
80	0.09	40	1600	1.11	200
115	0.07	40	2300	0.99	200
80	0.09	40	1600	0.56	100
150	0.05	40	3000	1.07	200
115	0.07	40	2300	0.75	150
150	0.09	40	3000	0.59	200

Figure 39. 3D printing parameter configurations for tap crown cylinders

Print results of tap crowns depicted heavy cracking in the printed samples. Due to this heavy cracking, the printed samples were deemed unsuitable for their friction welding with tap shanks as well as for their post-processing by grinding. This leads to unavailability of hybrid manufactured M16 taps in the following tapping tests. Therefore, tapping tests of the thesis work will be hereafter concentrated solely on standard M16 taps in order to validate utilized tapping torque in the numerical model. Print results of tap crown cylinders are highlighted in Appendix 5.

3 TESTING AND RESULTS

This chapter consists of experimental tapping tests and from their derived results conducted with standard M16 taps to validate the simplified FEM tapping simulation model's tapping torque used in the preceding design and topology optimization of M16 tap crown. An experimental setup constructed for carrying out the tapping tests is explained, with emphasis on utilized testing and measurement equipment as well as on enabled tapping conditions. Results of the tapping tests are studied in terms of effect of standard M16 tap type, workpiece material and cutting speed on the measured tapping torque with tapping performance of the standard M16 taps being compared in terms of tapping torque.

3.1 Experimental setup

Experimental tapping tests were conducted to measure and plot tapping torque of standard M16 taps. As detailed previously, due to unavailability of hybrid M16 taps resulting from their unsatisfactory 3D printing outcomes the tapping tests focused only on standard M16 taps unlike originally intended. Tapping tests were done using 35° spiral fluted M16 tap, and straight fluted spiral point M16 tap. As a preparation for their tapping, 14 mm through holes were drilled into 25 mm Al 6082 square bar workpieces and 20 mm S275JR square bar workpieces. Each aluminum and stainless-steel workpiece was cut to 15 cm in length, with 5 through holes in each cut workpiece. Tapping with M16 taps, and drilling of the through holes in preparation for tapping was conducted with Euroboor ECO.100/4D magnetic drilling machine. The drilling machine was clamped to a worktable separately for tapping and drilling using blanks for clamping in addition to its magnetic base. Workpieces were clamped using workbenches. Drilling machine setup with a tapped aluminum workpiece is seen below in figure 40.

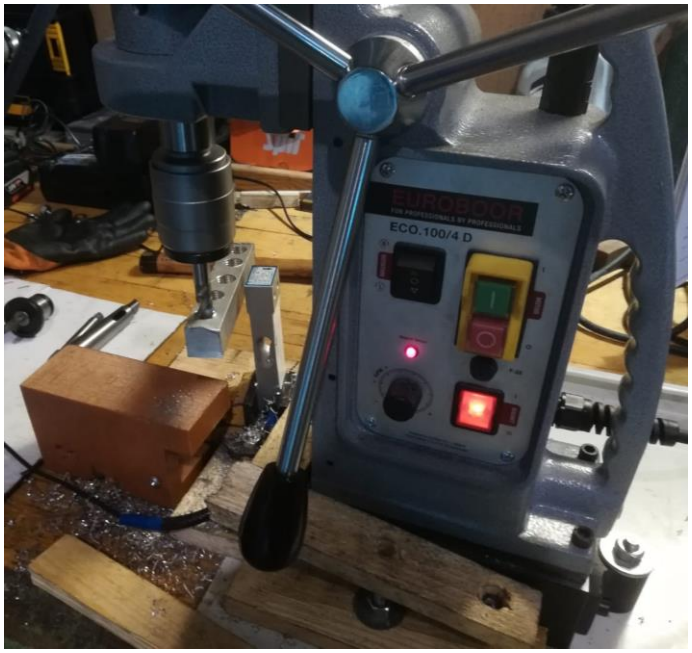

Figure 40. Euroboor ECO.100/4D drilling machine setup for tapping torque measurement

In order to measure and plot tapping torque while tapping the workpieces with given M16 taps, a set of electronic equipment was utilized. Jiuwu JJCP078 50 kg load cell sensor was clamped with a workbench to ensure its direct contact with a workpiece during its tapping to measure tapping torque as can be seen in figure 40. The load cell sensor was wired to HX711 load cell conversion module sensor which in turn was connected to Arduino UNO R3 microcontroller. Arduino was used to program the load cell sensor to measure tapping torque. Arduino Java script program measuring tapping torque with HX711 sensor is shown in Appendix 6. Measured tapping torque values were read from Arduino by using a Microsoft Excel add-on PLX-DAQ. PLX-DAQ provided a data acquisition system (DAQ) for collecting tapping torque values into an excel sheet, as well as for charting the tapping torque values. Electronics setup is shown below in figure 41, and utilized load cell electrical wiring with Arduino and HX711 are depicted afterwards in figure 42.

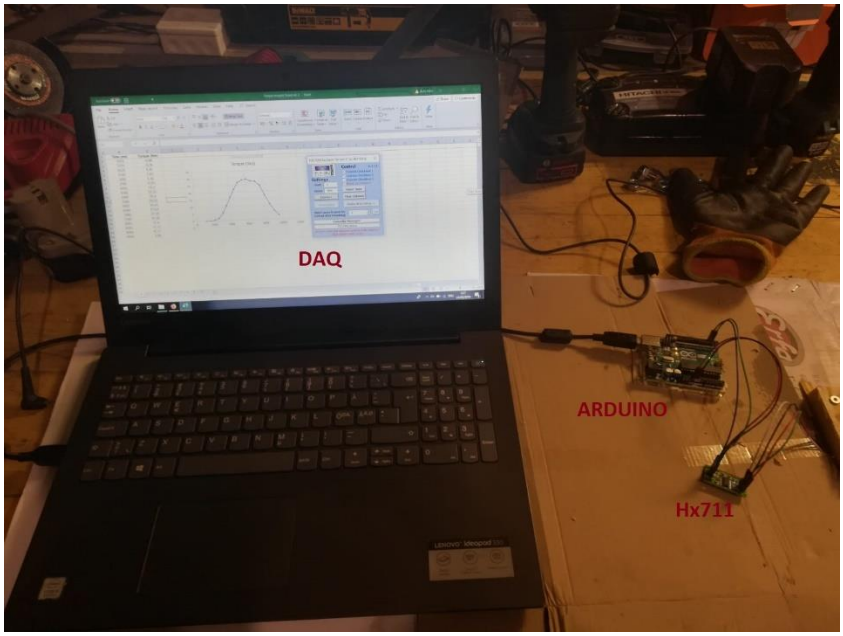

Figure 41. Electronics setup for tapping torque measurement

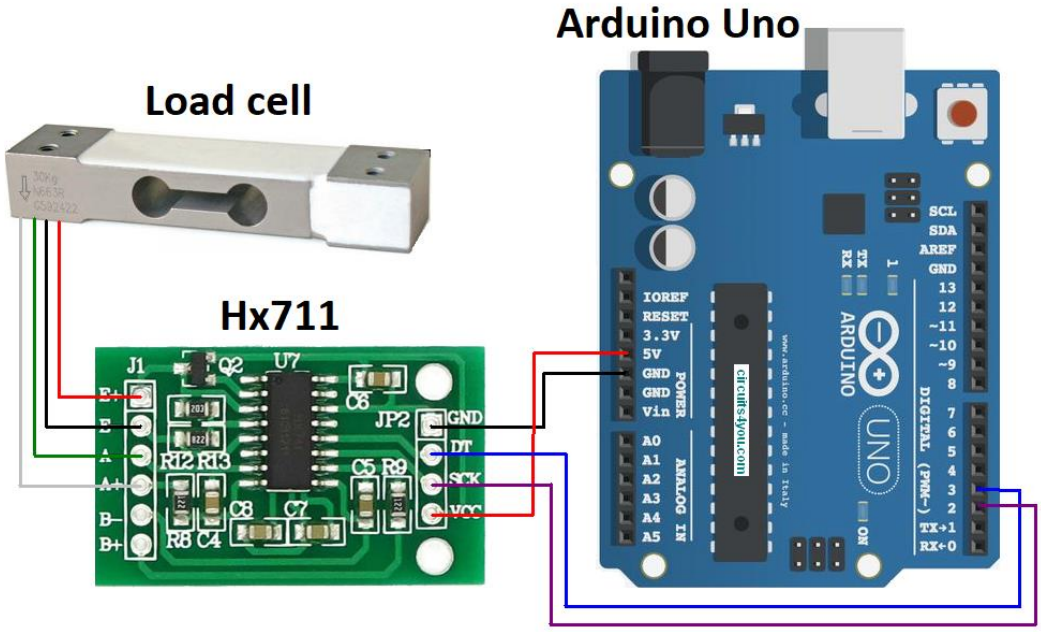

Figure 42. Load cell electrical wiring with HX711 and Arduino Uno (Mod. Circuits4you 2019).

Drilling of through holes into the workpiece was done while using WD-40 oil as a lubricant, whereas tapping had to be done in dry cutting conditions due to proximity of electronic equipment, and lack of effective lubricant collection system given resources of available testing center. Cutting speed configurations used in tapping were determined from 4-speed gearbox cutting speed values of the drilling machine, with 110 and 175 RPM being used in tapping. Only 110 RPM cutting speed was recommended for tapping with Euroboor ECO.100/4D. (Euroboor 2019, p. 14). Availability of workpiece material both for actual tapping tests, tapping trials as well as given time constraints restricted total number of tapped holes per cutting speed value, and per tested M16 tap. Used tapping test procedure is described below in table 4.

Table 4. Tapping test procedure with standard M16 taps

Standard M16 tap	Workpiece	Cutting speed	Tapped holes
Spiral fluted	Al	110 RPM	9
		175 RPM	7
	SS	110 RPM	10
		175 RPM	5
Straight fluted	Al	110 RPM	10
		175 RPM	7
	SS	110 RPM	10
		175 RPM	5

Jiuwu JJCP078 load cell has an accuracy class of C2, with its voltage output variation being ±0.15 mV. (Amazon 2019). Calibration of the load cell by inserting a known weight on it while reading its output through Arduino and HX711 resulted in output variation of ±0.030 kg, or ±0.029 N. Due to lack of available tools to allow torque calibration with a torque wrench in a given experimental setup, tapping torque measuring accuracy relies on the calibration done with the load cell using a known weight. Tapping torque was calculated as follows (equation 2).

$$M = F * r \quad (2)$$

Where in the given tapping torque equation F is tapping force applied upon load cell face in contact with the tapped workpiece, and r is distance to the load cell contact face from axis of rotation of the tap. Through holes were aimed at middle of each workpiece, and therefore distance was taken as 0.1 m for SS and 0.125 m for Al as seen in Appendix 6 about the utilized Java script. Time interval for measuring tapping torque was set as 0.5 s in the Java script.

3.2 Tapping torque with Al (aluminum) workpieces

Tapping torque measurements on Al workpieces were commenced with tapping trials. Tapping trials were conducted both with 110 and 175 RPM cutting speeds using straight fluted M16 tap. Tapping trials were done to validate if utilized electronics setup was working properly and whether outputted tapping torque results were reflective. After a successful tapping trial outcome, Al workpieces were tapped likewise firstly with straight fluted M16 tap on both used cutting speeds before continuing with spiral fluted M16 tap. Measured tapping torque plots of all tapped holes were averaged for a more reflective depiction of tapping torque and to exclude outliers and neglect unrealistic spikes within the measured values. Tapping torque plots for straight fluted M16 tap are displayed below in figures 43 and 44.

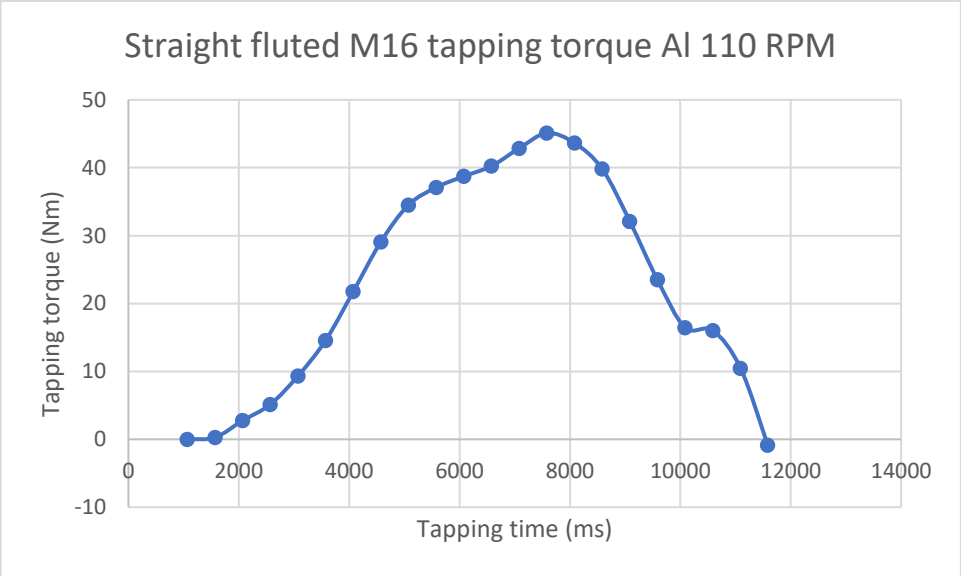

Figure 43. Tapping torque of straight fluted M16 tap with Al workpiece and 110 RPM cutting speed

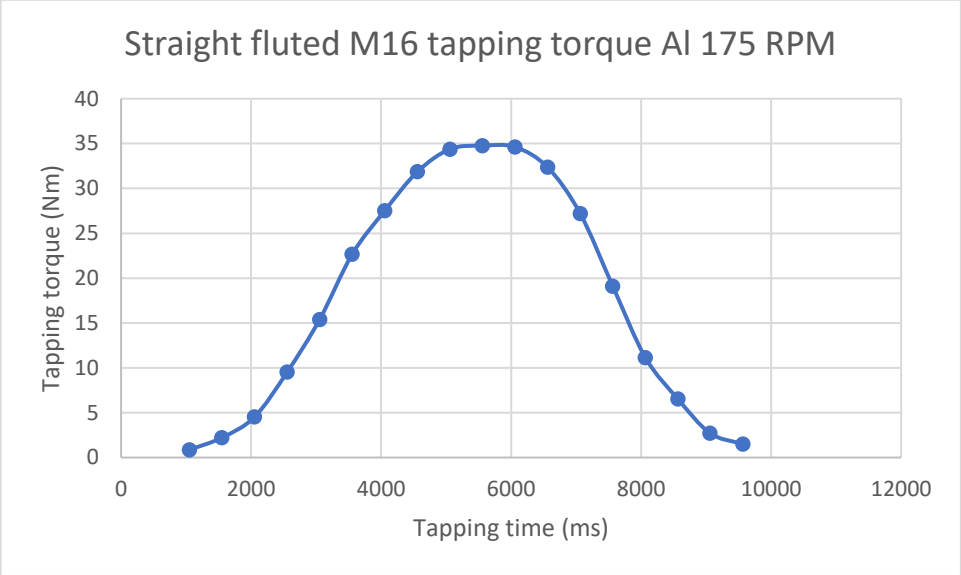

Figure 44. Tapping torque of straight fluted M16 tap with Al workpiece and 175 RPM cutting speed

After concluding tapping torque measurements with straight fluted tap, spiral fluted tap tapping torque measurements were conducted on Al workpieces. Similarly as with straight fluted tap, tapping torque plots of all tapped holes were averaged for displaying the tapping torque plots of spiral fluted M16 tap as is seen below in figures 45 and 46.

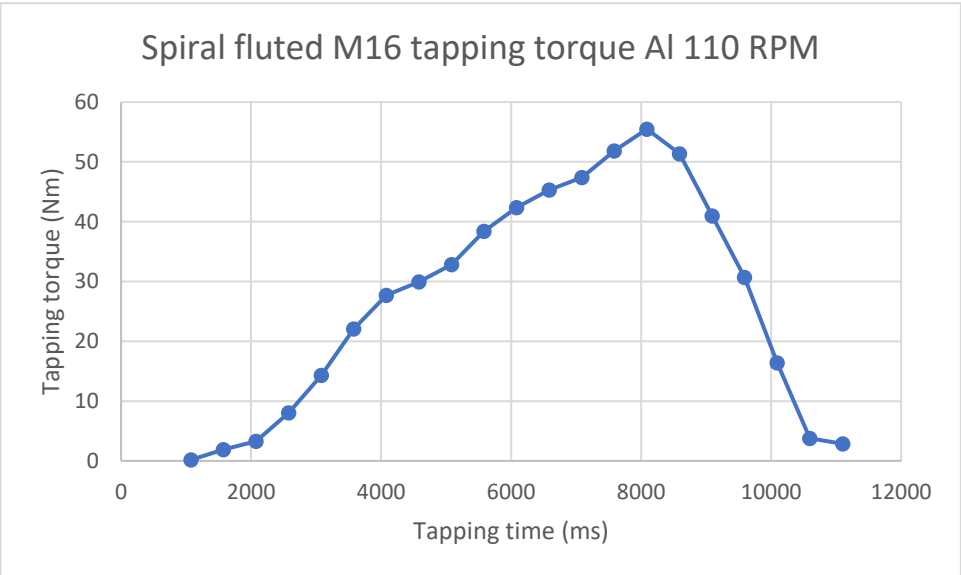

Figure 45. Tapping torque of spiral fluted M16 tap with Al workpiece and 110 RPM cutting speed

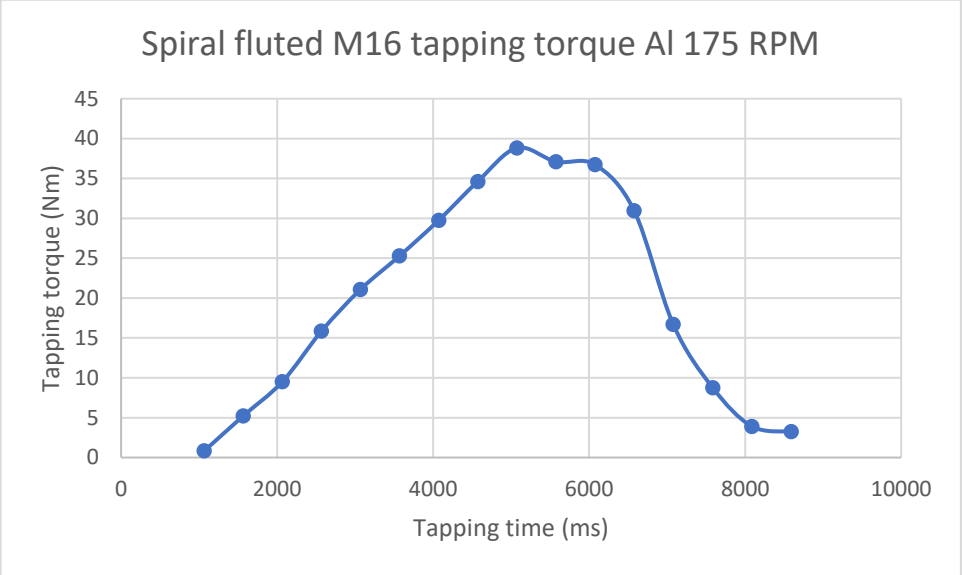

Figure 46. Tapping torque of spiral fluted M16 tap with Al workpiece and 175 RPM cutting speed

3.3 Tapping torque with SS (stainless-steel) workpieces

Much like with measuring tapping torque of Al workpieces, torque measurements on SS workpieces were commenced by tapping trials using the straight fluted M16 tap. Followed by a successful tapping trial, the tapping torque measurements on SS workpieces were done firstly with straight fluted tap and subsequently with spiral fluted tap. Like with tapping torque plots of Al workpieces, tapping torque plots of SS workpieces were averaged out of tapping torque plots of all tapped holes. Derived tapping torque plots of straight fluted tap with SS workpieces are seen next in figures 47 and 48.

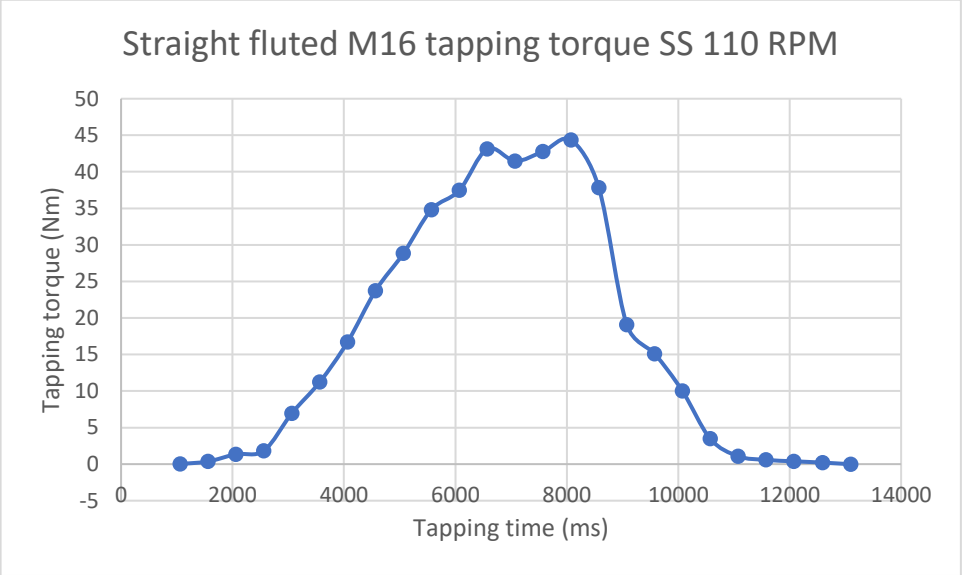

Figure 47. Tapping torque of straight fluted M16 tap with SS workpiece and 110 RPM cutting speed

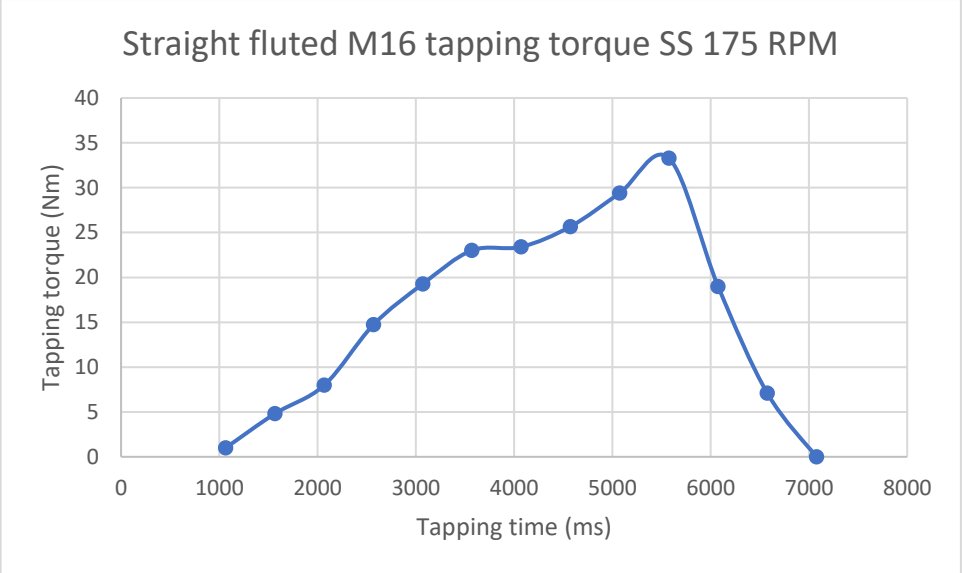

Figure 48. Tapping torque of straight fluted M16 tap with SS workpiece and 175 RPM cutting speed

As mentioned, tapping torque measurements on SS workpieces were conducted lastly with spiral fluted tap. As with other depicted tapping torque plots, derived tapping torque plot was averaged from measured tapping torque plots of all tapped holes on SS workpieces with the spiral fluted tap. Tapping torque plots of spiral fluted tap on SS workpieces are highlighted next in figures 49 and 50.

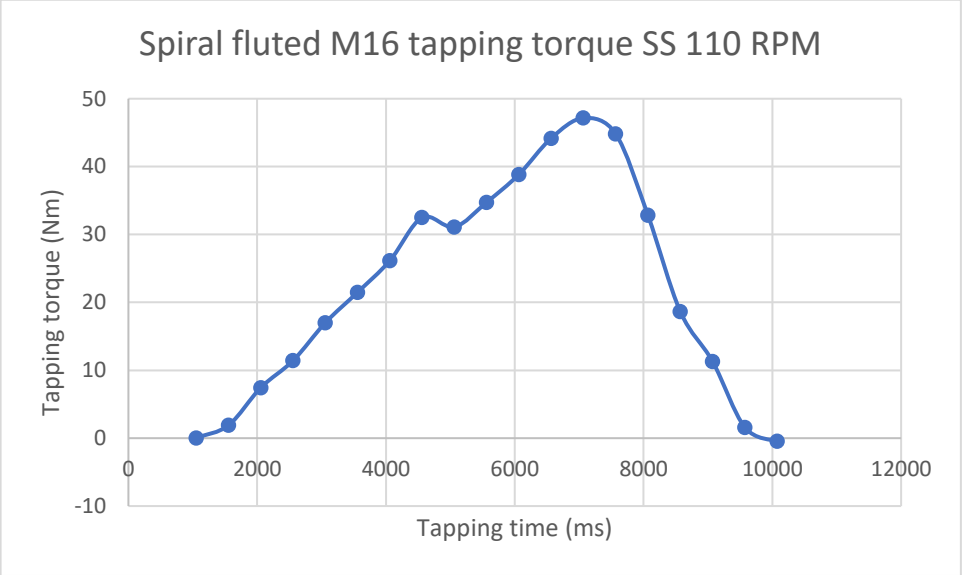

Figure 49. Tapping torque of spiral fluted M16 tap with SS workpiece and 110 RPM cutting speed

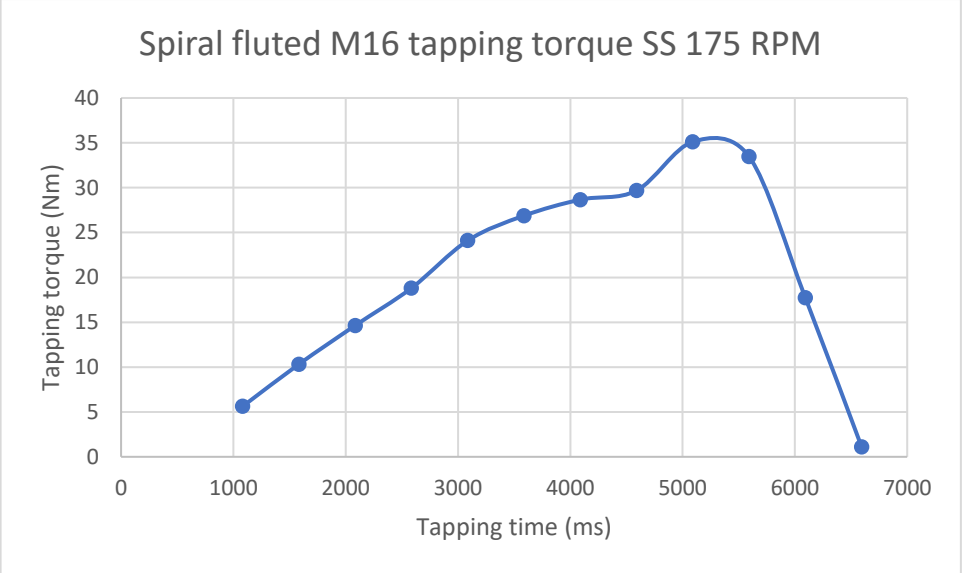

Figure 50. Tapping torque of spiral fluted M16 tap with SS workpiece and 110 RPM cutting speed

3.4 Tapping performance of straight fluted M16 tap

Derived tapping torque plots for straight fluted M16 tap are used to study how tapping performance is affected by altering cutting speed when tapping different workpiece materials. In case of straight fluted M16 tap, tapping torque plots depict a decrease in tapping torque when increasing cutting speed on both Al and SS workpiece materials as can be seen below in figures 51 and 52.

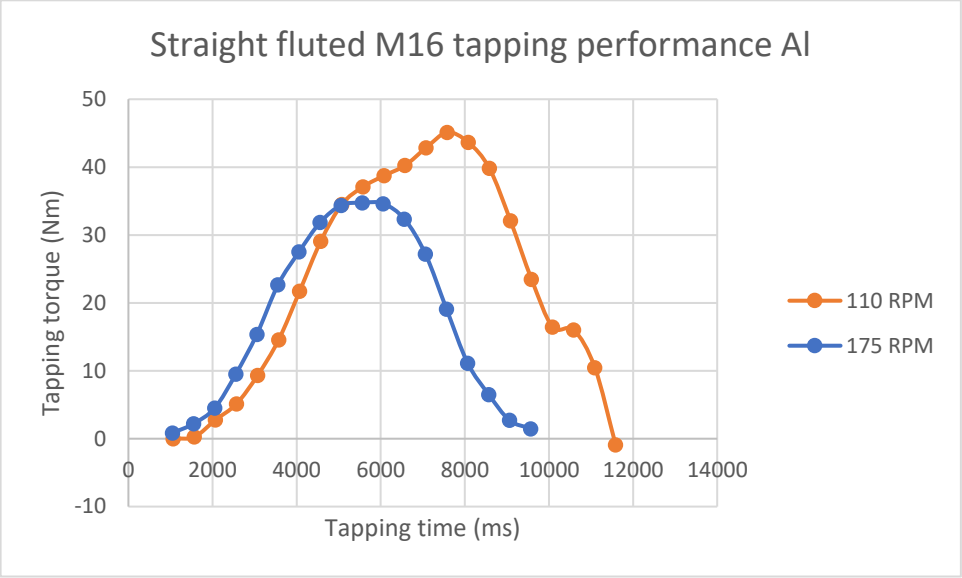

Figure 51. Tapping performance of straight fluted M16 tap with Al workpieces

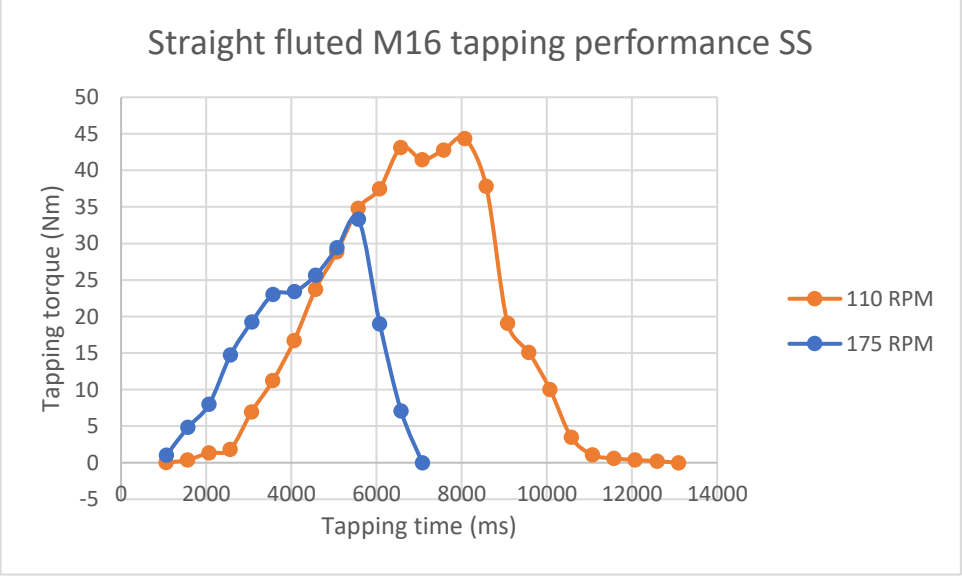

Figure 52. Tapping performance of straight fluted M16 tap with SS workpieces

When comparing tapping performance of straight fluted M16 tap per workpiece material on given cutting speed, it becomes apparent how tapping torque is slightly larger when tapping SS at 110 RPM. At 175 RPM however, derived tapping torque plots depict slightly larger tapping torque when tapping Al at 175 RPM. Results for tapping performance on a given cutting speed for straight fluted M16 tap are shown next in figures 53 and 54.

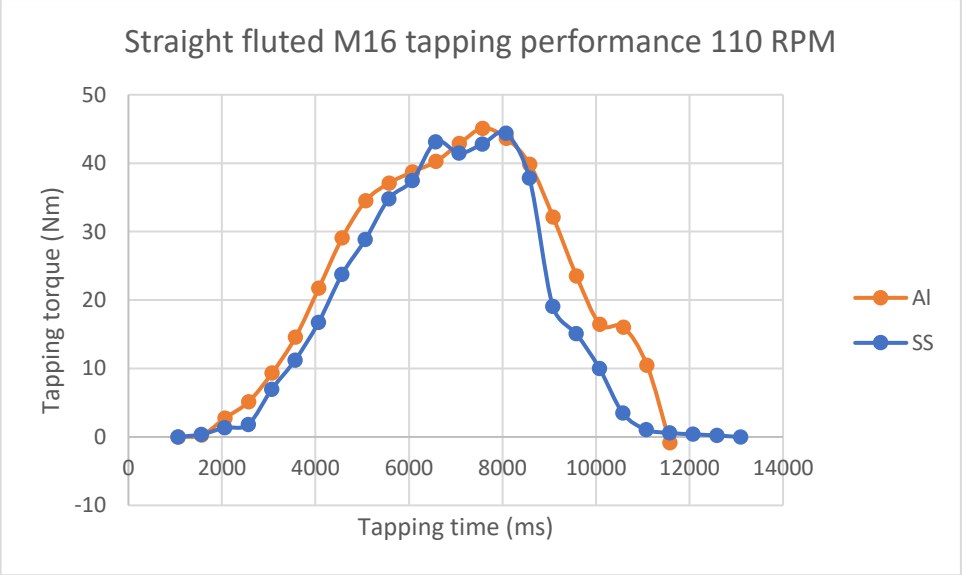

Figure 53. Tapping performance of straight fluted M16 tap with 110 RPM cutting speed

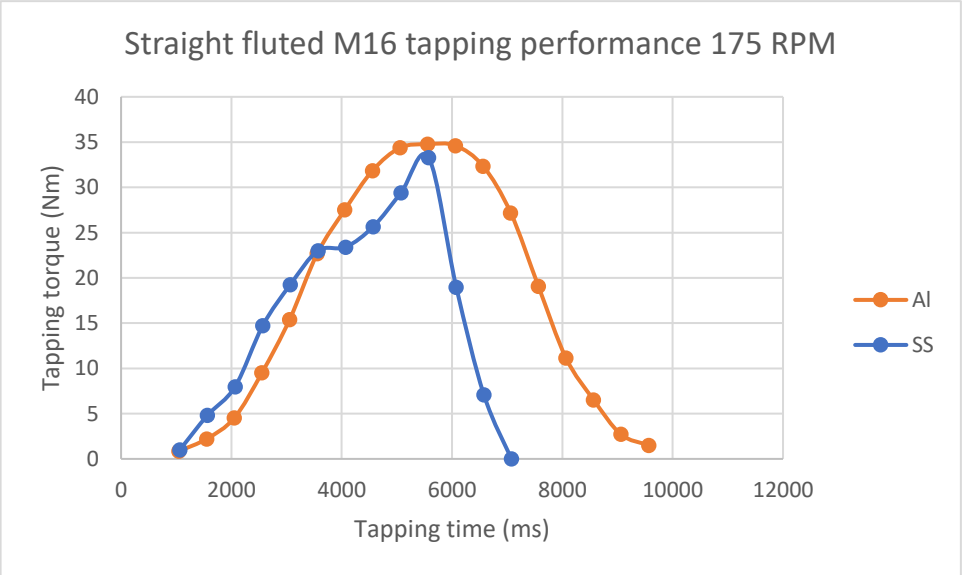

Figure 54. Tapping performance of straight fluted M16 tap with 175 RPM cutting speed

3.5 Tapping performance of spiral fluted M16 tap

As with straight fluted M16 tap, tapping performance of spiral fluted M16 tap depicts a decrease in tapping torque when increasing cutting speed. An increase in cutting speed likewise results in decreased tapping torque on both workpiece materials as can be noted below in figures 55 and 56 about tapping performance of spiral fluted M16 tap on Al and SS workpieces.

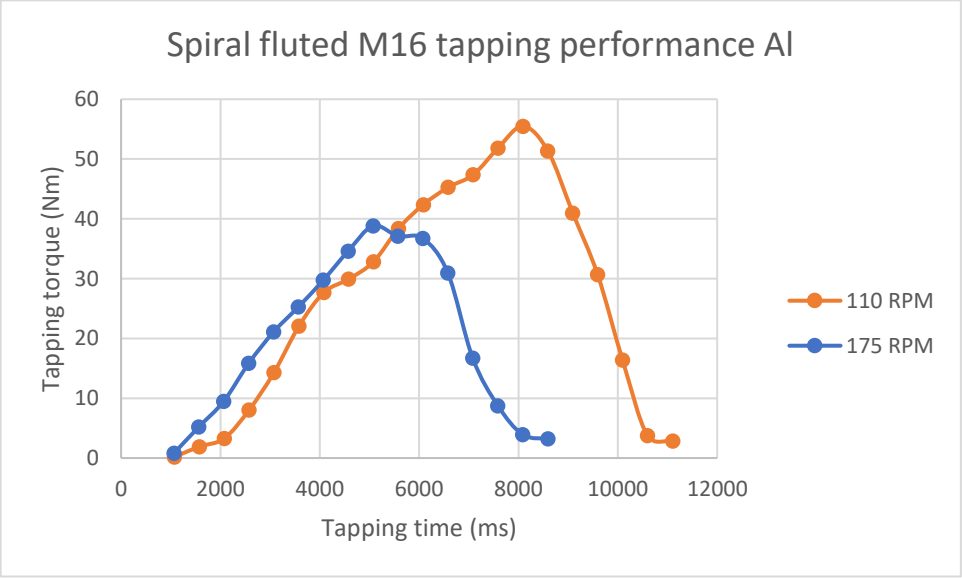

Figure 55. Tapping performance of spiral fluted M16 tap with Al workpieces

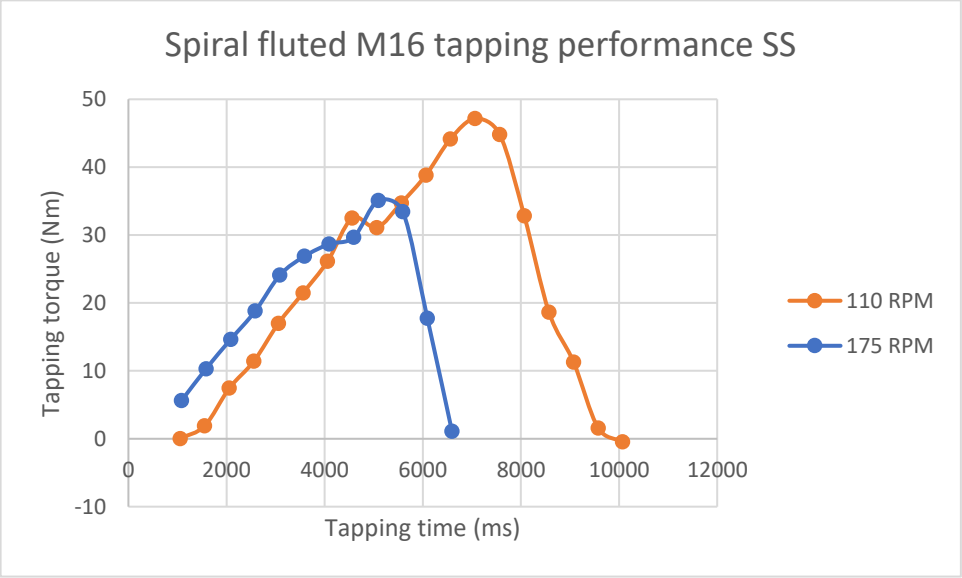

Figure 56. Tapping performance of spiral fluted M16 tap with SS workpieces

Observing tapping performance of spiral fluted M16 tap when accounting for cutting speeds depicts larger peak tapping torque values with Al workpieces on both utilized cutting speeds. However, initial tapping torque values result in larger torque values on SS workpieces with both cutting speeds as is seen below in figures 57 and 58.

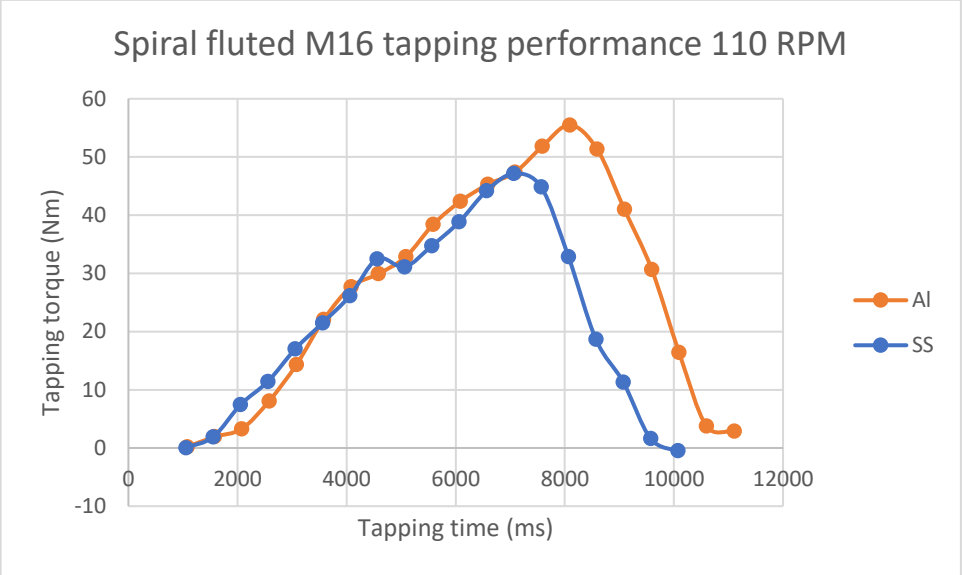

Figure 57. Tapping performance of spiral fluted M16 tap with 110 RPM cutting speed

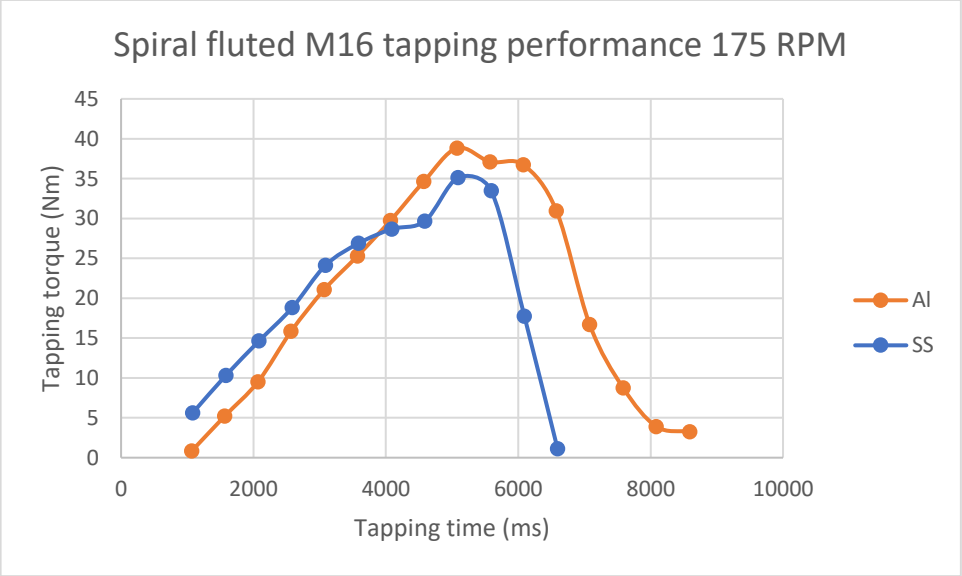

Figure 58. Tapping performance of spiral fluted M16 tap with 175 RPM cutting speed

3.6 Comparison of tapping performance

Tapping performance is compared between the tested M16 taps both on different workpiece materials as well as on the utilized cutting speeds with the workpiece materials. With Al workpieces, spiral fluted M16 tap show larger initial and peak tapping torque values on both cutting speeds as is displayed below in figures 59 and 60.

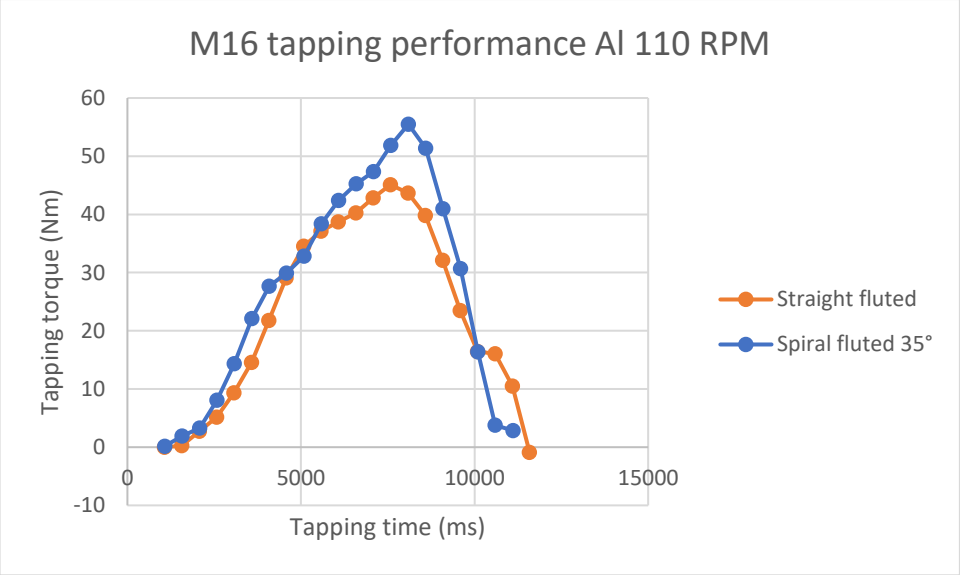

Figure 59. Tapping performance of M16 taps with Al workpieces and 110 RPM cutting speed

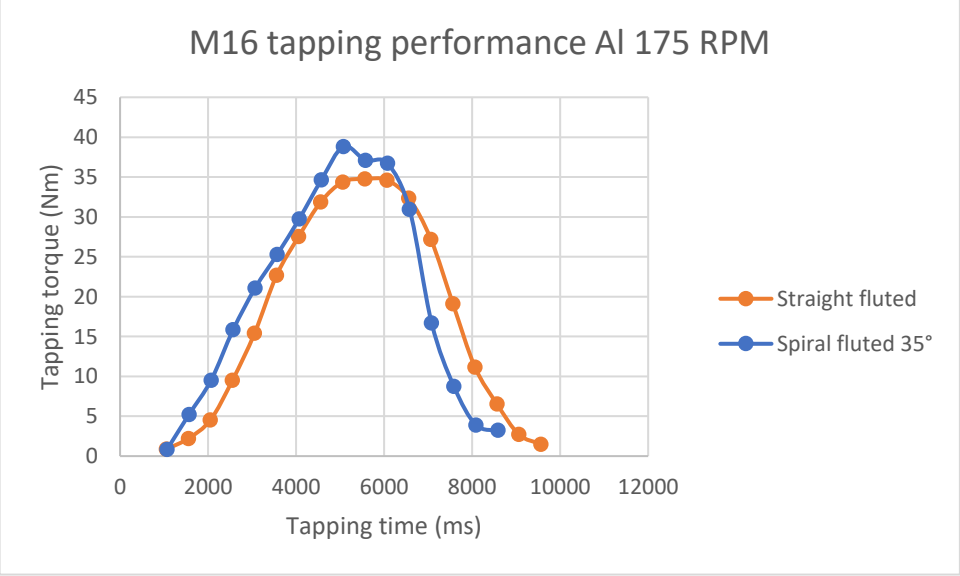

Figure 60. Tapping performance of M16 taps with Al workpieces and 175 RPM cutting speed

As with Al workpieces, derived tapping torque measurement results on SS workpieces depict larger initial and peak tapping torque values with spiral fluted M16 tap on both cutting speeds. Tapping performance comparison on SS workpieces with both cutting speeds on the tested M16 taps are displayed next in figures 61 and 62.

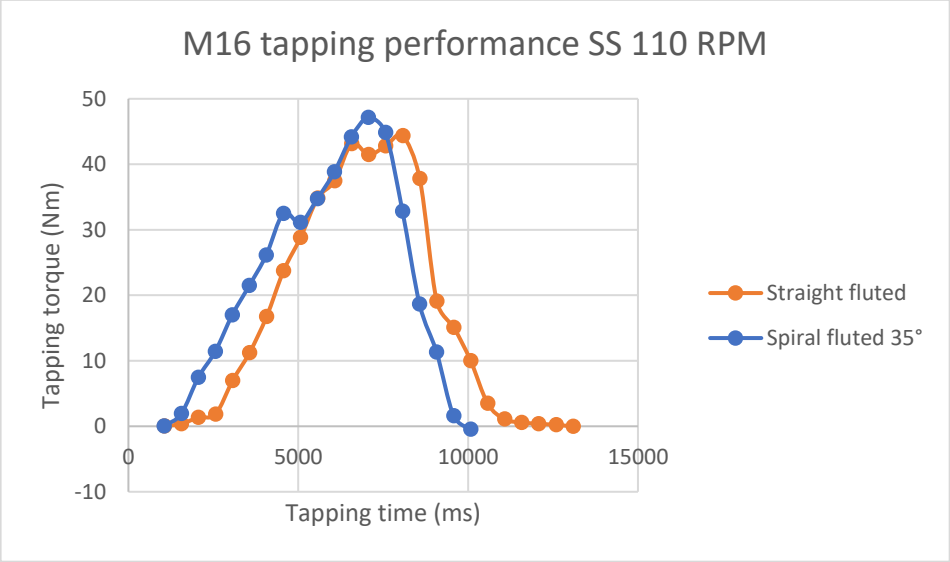

Figure 61. Tapping performance of M16 taps with SS workpieces and 110 RPM cutting speed

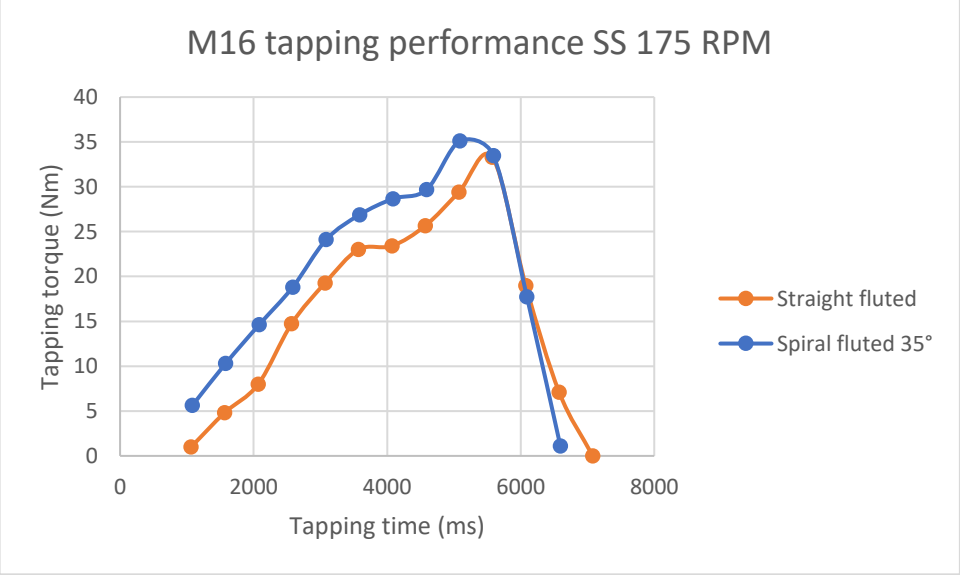

Figure 62. Tapping performance of M16 taps with SS workpieces and 175 RPM cutting speed

3.7 FEM model validation

For validating FEM model tapping torque value utilized in the simplified numerical tapping model of the thesis, total tapping torque values are derived from peak tapping torque of the displayed average M16 tapping torque plots in given tapping test configurations. Peak tapping torque was utilized to better reflect on required safety factor in would-be FEM tapping models when accounting for workpiece material and cutting speed. Derived total tapping torque values from the displayed tapping torque M16 plots are highlighted below in table 5.

Table 5. M16 standard tap derived total tapping torque values

Standard M16 tap	Workpiece	Cutting speed	Total tapping torque
Spiral fluted	Al	110 RPM	55 Nm
		175 RPM	39 Nm
	SS	110 RPM	47 Nm
		175 RPM	35 Nm
Straight fluted	Al	110 RPM	45 Nm
		175 RPM	35 Nm
	SS	110 RPM	44 Nm
		175 RPM	33 Nm

Utilized tapping torque in the FEM model was 40 Nm and it was derived from an industrial catalogue as a recommended tapping torque value when tapping workpiece material with tensile strength of 1000 MPa. Cutting speed was unaccounted in the catalogue's recommended tapping torque value for M16 tap. The FEM model tapping torque is subsequently compared with all derived total tapping torque values depicted above in table 5 to study how the FEM model tapping torque deviates from experimentally measured total tapping torque values according to tested M16 tap type, workpiece material and utilized cutting speeds. M16 tapping torque comparison between the tested M16 taps and the FEM tapping model is illustrated next in figure 63.

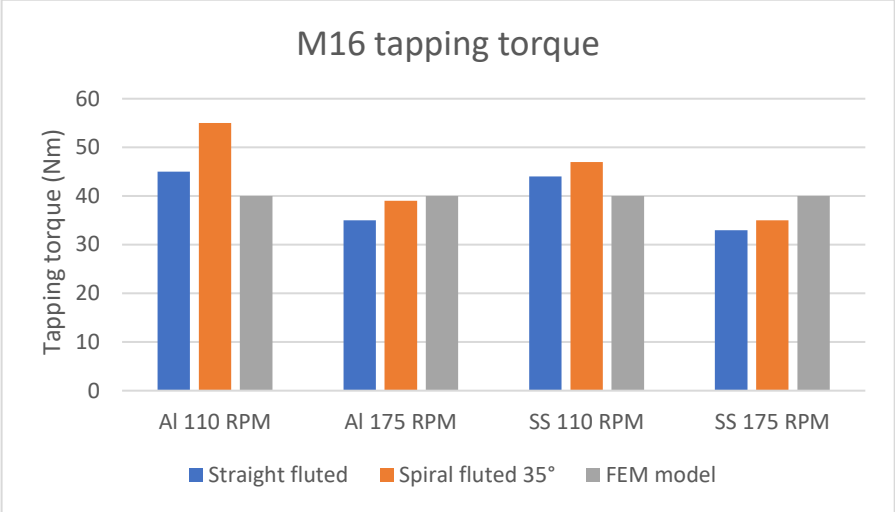

Figure 63. M16 tapping torque comparison between experimentally tested and numerically simulated M16 taps

Derived total tapping torque values depict highest deviation from the utilized FEM model tapping torque value with spiral fluted M16 tap when tapping Al workpieces at 110 RPM. Lowest deviation from the FEM model can be seen likewise with spiral fluted M16 tap when tapping Al workpieces at 175 RPM. Straight fluted M16 tap has smaller deviation from the FEM model tapping torque with both workpiece materials at 110 RPM whereas at 175 RPM spiral fluted M16 tap has smaller deviation from the FEM model tapping torque with both workpiece materials. FEM model tapping torque error from measured total tapping torque values is displayed below in table 6.

Table 6. M16 standard tap FEM model tapping torque error from total tapping torque

Standard M16 tap	Workpiece	Cutting speed	Total tapping torque	FEM model error
Spiral fluted	Al	110 RPM	55 Nm	-27 %
		175 RPM	39 Nm	+2 %
	SS	110 RPM	47 Nm	-15 %
		175 RPM	35 Nm	+14 %
Straight fluted	Al	110 RPM	45 Nm	-11 %
		175 RPM	35 Nm	+14 %
	SS	110 RPM	44 Nm	-9 %
		175 RPM	33 Nm	+21 %

4 DISCUSSION

Discussion of the thesis work is presented by firstly summing up how M16 tap optimization for 3D printing was carried out through its design and topology optimization. Key outcomes of the tap crown optimization are reflected on the results of both tap crown design, and topology optimization. Consequent 3D printing results for the design and topology optimized M16 tap crown samples are studied and contrasted to similar previous research. Provided experimental tapping conditions with the preceding experimental tapping tests are studied separately from the tapping test results which are studied thereafter. Lastly, adoption of 3D printed cutting tools in the industry is showcased for bearing in mind background of the thesis project.

4.1 M16 tap optimization for additive manufacturing

A simplified 3D FEM tapping model of this thesis work was utilized to firstly design optimize M16 tap by altering flute angle, rake angle, chamfer angle and chamfer length. The given tap parameters were altered while running static studies on the M16 tap upon applying tapping torque on its cutting edges to find optimal tap parameter resulting in lowest tap crown cross section stresses. Scale of impact in altering given tap parameters on the tap crown cross section stresses were found to be ascending in same order as the altered tap parameters were optimized, with flute angle having highest impact on tap crown stress distribution and chamfer length having smallest impact. Tap parameters differences between design optimized and standard M16 tap are highlighted below in table 7.

Table 7. M16 standard and design optimized tap parameter differences

M16 Tap configuration	Tap parameter			
	Flute angle	Rake angle	Chamfer angle	Chamfer length
Standard	45°	12°	18°	2 threads
Design optimized	40°	12°	18°	2 threads

Experimental validation for design optimization of M16 tap was to be indicated by comparing design optimized and hybrid manufactured M16 tap to standard M16 tap in the tapping tests. Due to printing results with optimized M16 tap crowns, this experimental validation could not be conducted. However, impact of flute geometry in M16 tapping performance was partially validated in the tapping tests with standard M16 taps. In the conducted experimental tapping tests with standard M16 taps, tapping performance was compared between standard spiral fluted 35° M16 tap and straight fluted spiral point M16 tap. Tapping performance comparison between the tested M16 taps validate flute geometry as having notable impact on experimentally measured tapping torque much like flute geometry had notable impact on tap crown stress distribution in the FEM model results during M16 design optimization.

The 3D FEM tapping model was secondly utilized to topology optimize M16 for its additive manufacturing. Several requirements were found to affect topology optimization of M16 tap crown. These were found to be 3D printability, tapping performance preservation, tap crown exterior margins, friction welding tolerance and metal powder release after 3D printing. Again, due to 3D printing results of the topology optimized tap crowns, topology optimization could not be validated by experimental tapping tests with hybrid manufactured M16 taps.

Comparison of tapping performance between standard M16 taps and hybrid manufactured M16 tap would have been needed to not only validate whether the hybrid manufactured M16 enabled reduced tap material usage whilst providing satisfactory tapping performance but to also experimentally validate the utilized safety value for tap crown cross section stresses during the M16 topology optimization. Testing of hybrid manufactured M16 taps with the chosen topology configurations for 3D printing in this thesis work are expected to be tapping tested at a later stage, after the thesis project, at Thurmer. Safety value for tap crown cross section stresses utilized in topology optimization is likewise expected to be under further consideration at Thurmer depending on future tapping test results with the hybrid manufactured M16 taps.

Topology optimization results indicate of larger tap crown cross section stress distribution with internal pentagon grid structure in comparison with internal hexagon grid structure even as tap crown mass reduction is relatively similar. This has been noted before in literature by Banicuk, Ragnedda and Serra (2002) when considering pure bending and comparing how number of sides in a polygon affects stress distribution as shown lastly in figure 64. Both the topology optimization results depicted in Appendix 4, as well as previous literature by Banicuk, Ragnedda and Serra (2002) depict hexagon as having smaller stress distribution compared to pentagon due to its larger torsional rigidity. With internal circle and square grid structures similar conclusions are difficult to derive as with internal square grid structures the tap crown mass reduction is relatively smaller whereas with internal circle grid structures tap crown cross section stresses could not be depicted due to mesh failures with utilized CAD software.

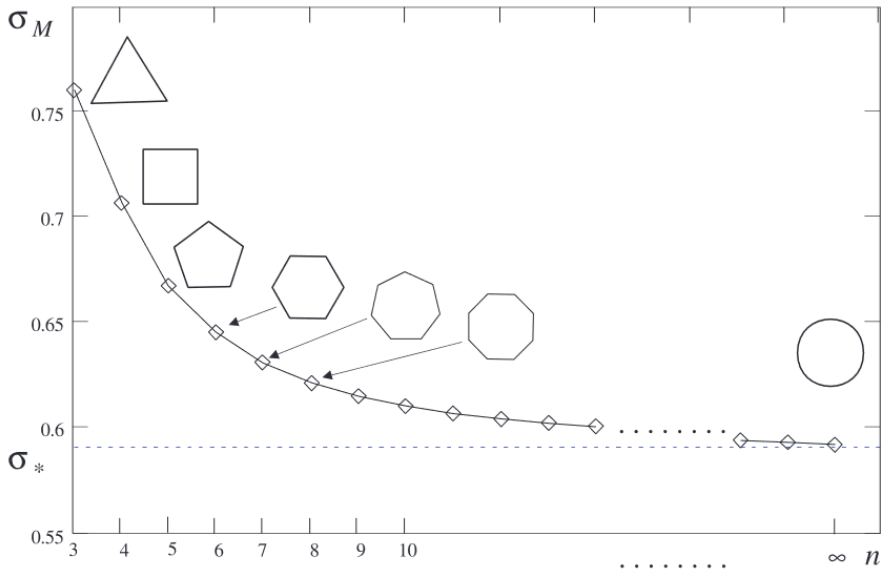

Figure 64. Stress distribution by number of sides in a polygon (Mod. Banicuk, Ragnedda and Serra 2002, p. 227).

4.2 3D printing outcomes with optimized M16 tap crowns

Selective laser melting of HSS T15 tap crown cylinders lead to heavy cracking as stated previously and depicted in Appendix 5. Both cracks and lack of fusion were revealed to have occurred in the preceding test prints with T15 samples. Combining an additive manufacturing technique like SLM with HSS as printing material has been noted as potentially crack inducing in the literature by Kempen et al. (2014). High hardness and low ductility, as with HSS T15, in connection to SLM results in high residual thermal stresses. The thermal stresses, illustrated next in figure 65, can be caused during melting of a print layer right below it due to compressive stresses between expanding upper melt layer and cooler lower layer, or on top layers during their cooling due to tensile stresses between shrinking upper melt layer and cooler lower layer. (Kempen et al. 2014, p. 131-133).

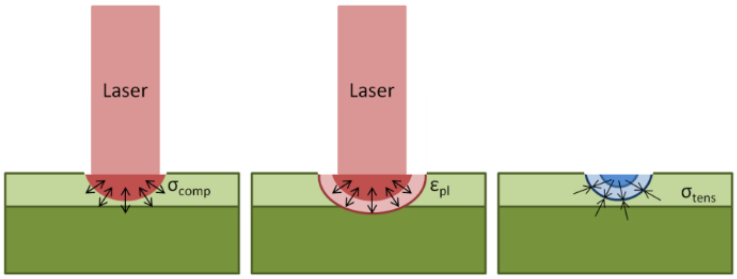

Figure 65. Illustrated thermal stresses in SLM of HSS T15 (Mod. Kempen et al. 2014, p. 133).

R&D project partner of Thurmer responsible for 3D printing of the optimized tap crowns noted as one potential cause for heavy cracking having been a too low platform temperature for a tool steel, 170°, as pre-heating of build chamber platform is used to reduce thermal stresses present in SLM of HSS T15. However, comparison between 3D printing results of HSS T15 tap crown cylinders with 3D printed HSS M2 samples from the literature by Kempen et al. (2014) depicts less cracking and lack of fusion with a mere pre-heating temperature of 90°C. Example of selectively laser melted HSS M2 part with pre-heating temperature of 90°C is seen next in figure 66.

Figure 66. HSS M2 part 3D printed by SLM with pre-heating platform temperature 90°C (Mod. Kempen et al. 2014, p. 134).

Reasons for heavy cracking of HSS T15 by SLM is likely a combination of many SLM process parameters in addition to the utilized platform temperature. As mentioned, several 3D printing parameters were configured for final 3D printing of tap crown cylinders. These were laser power, scanning speed, hatch distance, laser exposure time and point distance. Previous literature indicates of too low laser power in SLM causing lack of fusion as per Zhang, Li and Bai (2017). Likewise, utilizing high scanning speed with low laser power can lead to lack of fusion. Low scanning speed with high laser power on the contrary can lead to porosity defects. (Zhang, Li and Bai 2017, p. 517-519).

For producing successful HSS T15 prints by SLM, more extensive trials need to be continued by configuring the printing parameters. These trials should consider all possible SLM process factors for heavy cracking and lack of fusion in the 3D printed samples whether they were to be laser, scanning, powder or temperature related. Different process factors necessary to consider in SLM of HSS T15 are depicted next in figure 67.

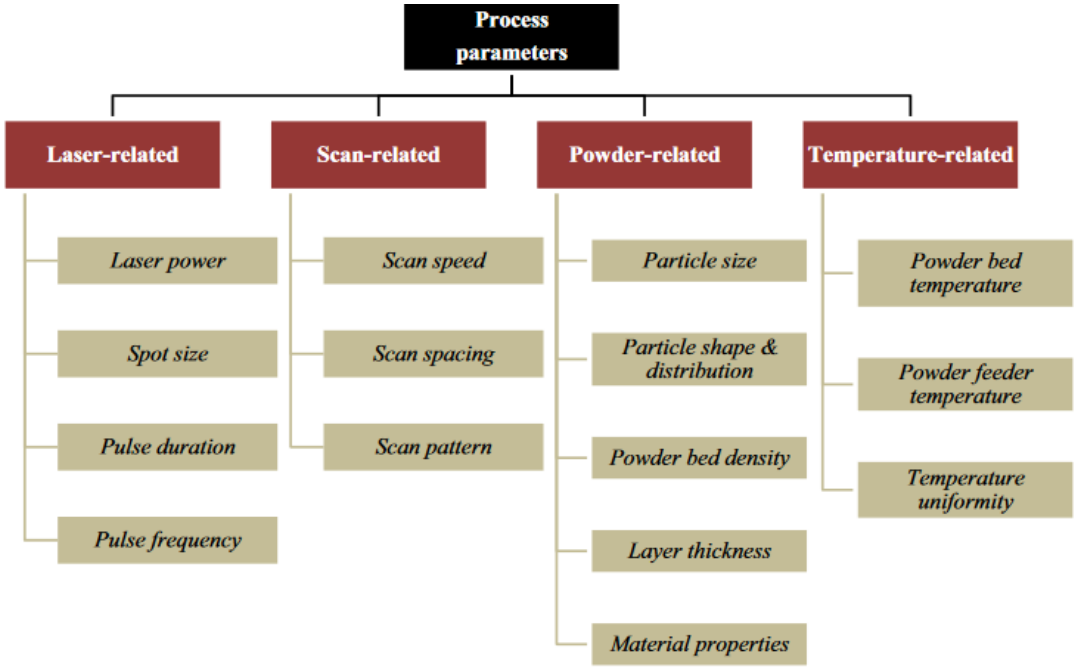

Figure 67. SLM process factors to consider for eliminating cracking in HSS T15 samples (Mod. Aboulkhair et al. 2014, p. 78).

4.3 Experimental tapping test conditions

As hybrid manufactured M16 taps could not be made available for tapping performance tests due to their 3D printing outcomes described previously, the tapping tests were instead carried out with standard M16 taps. Utilized magnetic drill in combination with the given electronic equipment setup provided reflective outputs from tapping torque measurements whereas the setup and clamping of the load cell with the tapped workpieces provided a set of possible errors into the measured tapping torque values.

Contact between load cell and tapped workpiece had a bottom support frame for the workpiece only for tapping first few threads into the hole, after which the workpiece remained without a bottom support frame when it was in direct contact with the load cell during tapping. Not having a bottom support frame with the workpiece was disadvantageous for measuring tapping torque, as the weight of the workpiece tilted many of the holes while tapping them. This could be seen in many of the tapping torque plots for individual tapped holes regardless of workpiece material or cutting speed. Tapping torque plot for a tilted hole often revealed a notably higher tapping torque values, as the M16 standard tap would try to drill part of the hole which was unaligned. Lack of bottom support frame for the workpiece in utilized experimental setup is better illustrated next in figure 68.

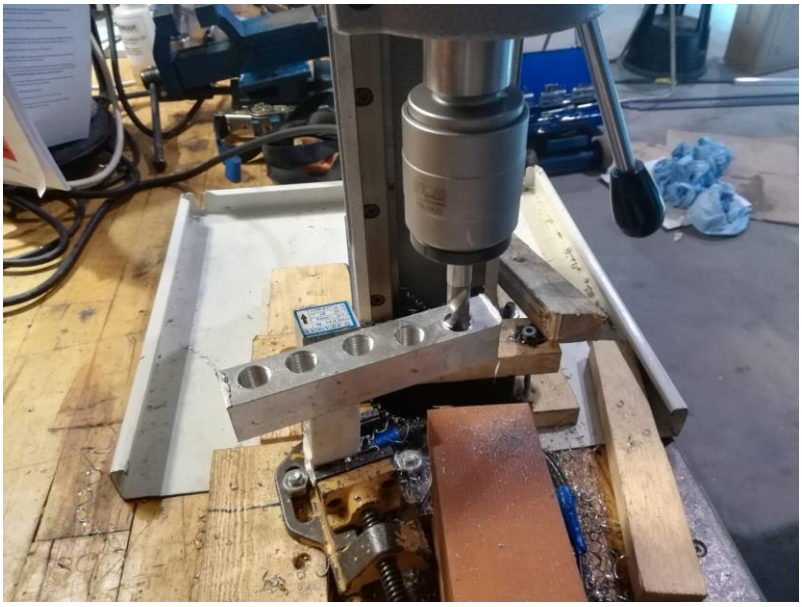

Figure 68. Lack of bottom support frame for a tapped workpiece in the experimental setup

Distance between load cell contact surface and tapped hole's axis of rotation varied slightly among the workpieces despite aiming all through holes to the midpoint of each cut workpiece square bar. The workpieces had been firstly drilled with bottom holes, before the bottom holes were drilled into through holes. Bottom holes were drilled into the workpieces initially due to intention of tapping them instead of through holes with the tested standard M16 taps. This idea was abandoned after confirming a lack of proper clamping system for workpieces with bottom holes and used drilling machine. Drilling of bottom holes caused a slight variation in the hole location due to proximity with the magnetic base of the drilling machine causing workpiece movement within workbench while drilling. Workpiece hole location variation and drilling setup are depicted next in figures 69 and 70.

Figure 69. Workpiece hole location variation

Figure 70. Drilling setup

Tapping of the workpieces had to be done without any lubricant due to lack of lubricant collection system, as well as proximity with electronic measuring equipment. Dry cutting conditions increased measured tapping torque values, and affected chip formation during tapping. Chip collection was conducted only after finishing the tapping procedure, which increased likelihood of a recently tapped hot chip burning an electric jumper wire, dismembering electrical connection between the load cell, HX711 and Arduino. Proximity of the load cell strain gauge body with exiting chips also risked damage from the exiting chips to the protective material around the strain gauges of the load cell.

Clamping of used drilling machine, load cell as well as workpieces in Thurmer's testing center requires more consideration before further testing as the current clamping systems of the experimental setup cannot withstand tapping torque with bottom holes. Moreover, as the current experimental setup may cause a higher tapping torque value from reasons described previously, using it with hybrid manufactured taps results in significant risk of tap breakage. Tapping a bottom hole in the current experimental setup at a minimum cutting speed, 10% of 110 RPM, with a standard M16 straight fluted spiral tap resulted in tap breakage.

4.4 Tapping performance test results with standard M16 taps

Tested standard M16 taps display lower tapping torque values on both workpiece materials when cutting speed was increased. Spiral fluted M16 tap is seen as having higher tapping torque and shorter tapping time in comparison with straight fluted spiral point M16 tap on both workpiece materials and cutting speeds. Spiral point flute geometry pushes chips forward in tapping direction allowing for their evacuation, which reduces tapping torque as fewer chips will accumulate on the tap flute during tapping. Spiral flute geometry provides a faster tapping process as spiraling flute pulls chips against tapping direction from the way of the tapped threads, but as chips accumulate on the spiral flute it increases tapping torque.

Decrease in tapping torque with increase of cutting speed has been previously recorded in literature by Uzun and Korkut (2016). This is due to higher cutting speed providing a more continuous tapping process. During a more continuous tapping process, chips cannot accumulate into the tapped hole. Higher cutting speed causes consequently increases heat generation, which facilitates tapping of workpiece in its cutting area. (Uzun and Korkut 2016, p. 277-278).

With straight fluted M16 tap at 110 RPM, tapping torque values are relatively similar both with Al and SS. At 175 RPM cutting speed on the contrary tapping time is notably smaller and tapping torque is relatively smaller with SS workpiece. This is due to SS being harder material than Al, thereby producing shorter chips. Shorter chips will not result in chips piling up on the tap flute during tapping which reduces tapping torque, and shorter chips are faster to evacuate which makes the tapping process faster.

Observing from measurements of spiral fluted M16 tap both at 110 RPM and 175 RPM, tapping time as well as tapping torque is smaller with SS. Initial tapping torque values are however depicted larger with SS due to chips accumulating on the spiral flute of the tap. As Al has longer chips, their evacuation from the spiral flute takes longer, which increases both tapping time and torque due to chip accumulation on the tap spiral flute.

Without experimental testing of hybrid manufactured and design optimized M16 taps, found 3D FEM tapping simulations about tap parameter effect on tapping performance in the literature review as well as utilized simplified 3D FEM tapping simulation could not be validated. However, tapping performance results for spiral point and spiral fluted 35° standard M16 tap depict relatively small deviation when comparing measured total tapping torque values to the utilized tapping torque with the 3D FEM tapping model of the thesis work.

4.5 Industrial adoption of additive manufactured cutting tools

Limited amount of commercial additive manufactured milling cutters and drill bits can be found from industry. 3D printing of taps is very much still in early stages as has been showcased in this thesis work. Like with Thurmer, thread cutting tool manufacturers have yet gone past prototyping and testing of 3D printed taps. Examples of other additive manufactured cutting tools like milling cutters and drill bits can be found from German-based cutting tool manufacturers Komet Group and MAPAL Inc. Komet Group has 3D printed milling cutters which have both internal cooling channels for a better coolant flow, optimized design for cutting edges to allow a more effective milling process and optimized design for cutting edge holder for weight reduction. (Komet Group 2019). Figure 71 below depicts one 3D printed milling cutter from Komet Group.

Figure 71. Commercial additive manufactured milling cutter (Mod. Komet Group 2019).

MAPAL Inc., another German-based cutting tool manufacturer as previously mentioned, has developed insert drills in which AM produced drill insert and insert holder are combined with conventionally manufactured drill shank. AM allows use of smaller internally cooled insert drills as previously the small size of an insert drill prevented use of cooling channels when the drills were produced conventionally. The 3D printed insert drills are designed for optimal chip removal and formation in the drill insert, enhanced coolant flow through the drill insert and cost reductions in the insert holder drill body. Figure 72 below showcases a 3D printed insert drill from MAPAL Inc. (MAPAL Inc. 2019.)

Figure 72. Commercial additive manufactured insert drill (MAPAL Inc. 2019).

5 CONCLUSIONS

A systematic approach for designing an optimized M16x2 thread tap crown for additive manufacturing has been laid out in this thesis work. The approach involves altering of tap parameters in design optimization of the M16 tap and meeting all recognized requirements for topology optimization of the M16 tap. Altering of tap parameters in the utilized numerical tapping simulation model of the thesis work depicted tap flute angle as having highest impact on stress distribution along M16 tap crown cross sections. Topology optimization of the tap resulted in internal hexagon grid structure and internal hollow structure as being most capable topology configurations for reducing tap mass whilst upkeeping satisfactory tap crown stress distribution, justifying their selection for 3D printing.

3D printing outcomes of design and topology optimized M16 tap crowns produced samples with heavy cracking, as well as lack of fusion. As a consequence, instead of carrying out experimental tapping performance tests on the hybrid manufactured M16 taps in which the 3D printed optimized tap crown samples would have been joined with conventionally manufactured tap shanks by friction welding, the tapping tests were conducted on standard M16 taps.

The tapping tests derived tapping torque plots for 35° spiral fluted and straight fluted standard M16 taps. Tapping performance results on the tested M16 taps with 110 and 175 RPM cutting speeds as well as Al and SS workpieces depicted tapping torque values as decreasing with an increase in cutting speed, which was found to be in good agreement with previous studies from the literature. Tapping torque results in comparison with utilized tapping torque in the FEM model of the thesis work showed relatively small deviation, and comparison of tapping performance among workpiece materials and among M16 tap flute type were likewise found to be aligned with previous research.

This thesis work is a living proof of a fast-paced trend in the cutting tools industry in which cutting tools manufacturers small and big alike are seeking new solutions to old problems from the promise known as additive manufacturing, or 3D printing. Thurmer, the commissioner of this thesis project, can therefore be seen as an exemplary SME company with bold and broad-minded future vision, one in which additive manufacturing can drastically disrupt traditional products, both in their design as well as manufacturing.

Adoption and exploitation of additive manufacturing holds tremendous potential for cutting tools such as taps as it can allow reduction in material usage and production time while increasing tool life and improving tool performance. It provides a clear way forward, towards more sustainable, economical and effective future of cutting tools. Future vision on the impact of additive manufacturing on cutting tools can be best summed up in figure 73 below about a 3D printed thread gauge of Thurmer.

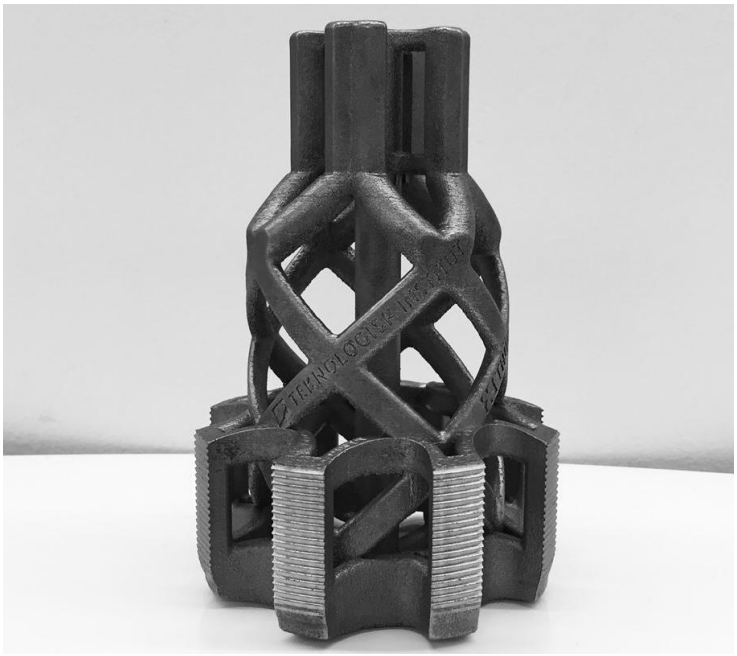

Figure 73. Additive manufactured thread gauge, 90% mass reduction

REFERENCES

Amanullah, A., Murshiduzzaman, Saleh, T., Khan, R. 2017. Design and Development of a Hybrid Machine combining Rapid Prototyping and CNC Milling Operation. Procedia Engineering. Vol 184, p. 165-169

Amazon. 2019. Product decription. [Web document] [Referred: 27.05.2019] Available: https://www.amazon.com/Platform-Scale-Weighting-Electronic-Balance/dp/B00NH9Q9LK

Amoulkhair, T., Everitt, M., Ashcroft, I., Tuck, C. 2014. Reducing porosity in AlSi10Mg parts processed by selective laser melting. Additive manufacturing. Vol 1-4, p. 78

Astakhov, V., Outeiro, J. 2008. Metal Cutting Mechanics, Finite Element Modelling. Springer. Machining, p.13

Banicuk, N., Ragnedda, F., Serra, M. 2002. Optimum shapes of bar cross-sections. Structural and Multidisciplinary Optimization. Vol 23, p. 227

Black, J., Kohser, R. 2012. DEGARMO'S MATERIALS and PROCESSES in MANUFACTURING. Wiley. Courier Graphics-Kendallville, p. 1181-1190
DORMER. 2013. Technical Handbook, p. 23-67

Circuits4you. 2019. Load Cell connections to HX711 and Arduino. [Web document] [Referred: 28.05.2019] Available: https://circuits4you.com/2016/11/25/hx711-arduino-load-cell/

Du, W., Bai, Q., Zhang, B. 2016. A Novel Method for Additive/Subtractive Hybrid Manufacturing of Metallic Parts. Procedia Manufacturing. Vol 5, p. 2-3

Euroboor. 2019. USER MANUAL ECO.100/4D Magnetic Drilling Machine, p. 14

Fanar. 2018. Tools for threads, p. 239-256

Ghani, S., Zakaria, M., Harun, W., Zaulkafilai, Z. 2017. Dimensional accuracy of internal cooling channel made by selective laser melting (SLM) and direct metal laser sintering (DMLS) processes in fabrication of internally cooled cutting tools. MATEC Web of Conferences. Vol 90, p. 2-3

Herzog, D., Seyda, V., Wycisk, E., Emmelmann, C. 2016. Additive manufacturing of metals. Acta Materialia. Vol 117, p. 371-372

ISO 13399-1:2006. 2019. Cutting tool data representation and exchange – Part 1: Overview, fundamental principles and general information model. [Web document] [Referred: 18.01.2019] Available: https://www.iso.org/obp/ui/#iso:std:iso:13399:-1:ed-1:v1:en

ISO/ASTM 52900:2015. 2019. Additive manufacturing – General principles – Terminology. [Web document] [Referred: 17.01.2019] Available: https://www.iso.org/obp/ui/#iso:std:iso-astm:52900:ed-1:v1:en

ISO/TS 13399-50:2013. 2019. Cutting tool data representation and exchange – Part: 50: Reference dictionary for reference systems and common concepts. [Web document] [Referred: 18.01.2019] Available: https://www.iso.org/obp/ui/#iso:std:iso:ts:13399:-50:ed-2:v1:en

Kempen, K., Vrancken, B., Buls, S., Thijs, L., Humbeeck, J., Kuth, J. 2014. Selective Laser Melting of Crack-Free High Density M2 High Speed Steel Parts by Baseplate Preheating. Journal of Manufacturing Science and Engineering. Vol 136, p. 131-134

Komet Group. 2019. 3D-printed PCD milling cutters. [Web document] [Referred: 28.01.2019] Available:
http://www.kometscandinavia.com/images/Komet_kataloger/1342CF11-9F85-4819-AD2A-17AF4F0A7AF9webspeed.dk.pdf

Kurzynowski, T., Chlebus, E., Kuznicka, B., Reiner, J. Parameters in Selective Laser Melting for processing metallic powders. High Power Laser Materials Processing: Lasers, Beam Delivery, Diagnostics, and Applications. Vol 8239, p. 2

MAPAL Inc. 2019. Conventionally and additive manufactured QTD INSERT DRILL. [Web document] [Referred: 28.01.2019] Available: https://www.mapal.com/fileadmin/00_PDF-Dateien/Kataloge/en/Insert_drill_QTD-en.pdf

Mech4study. 2017. Friction Welding: Principle, Working, Types, Application, Advantages and Disadvantages. [Web document] [Referred: 15.03.2019] Available: http://www.mech4study.com/2017/04/friction-welding-principle-working-types-application-advantages-and-disadvantages.html

Muthu, S., Savalani, S. 2016. Handbook of Sustainability in Additive Manufacturing Volume 1. Springer. Environmental Footprints and Eco-design of Products and Processes, p. 3

Oberg, E., Jones, F., Horton, H., Ryfell, H., Heald, R. 2000. 26th Edition Machinery's Handbook. Industrial Press Inc, p. 873-874

Oezkaya, E., Biermann, D. 2017. Segmented and mathematical model for 3D FEM tapping simulation to predict the relative torque before tool production. International Journal of Mechanical Sciences. Vol 128-129, p. 697-707

Peng, F., Yan, X., Guo, H., Lu, L., Zhang, S., Li, J. 2016. Research on the Effects of Tapping Performances with Multiple-Type Parameters. Key Engineering Materials. Vol 693, p. 1114-1120

Radzevich, S. 2012. Dudley's Handbook of Practical Gear Design and Manufacture, Second Edition. CRC Press. Taylor & Francis Group, p. 79

Rayna, T., Striukova, L. 2016. From rapid prototyping to home fabrication: How 3D printing is changing business model innovation. Technological Forecasting & Social Change. Vol 102, p. 214-217

Renishaw. 2015. AM 400 additive manufacturing system, p. 1

Stoyanov, P. 2016. CUTTING TOOL MADE BY ADDITIVE MANUFACTURING. [Web document] [Referred: 24.01.2019] Available: https://patents.google.com/patent/US20160332236

Tang, Y., Han, R., Geng, L., Ju, B. 2011. Research on specific structural parameters of modified-tooth Tap for titanium alloy TC4. Applied Mechanics and Materials. Vol 66-68, p. 1286-1290

Thurmer. 2019. THÜRMER & CO. [Company website] [Referred: 04.02.2019] Available: http://www.thurmer.com/history/

Tofail, S., Koumoulos, E., Bandyopadhyay, A., Bose, S., O'Donoghue, L., Charitidis, C. 2018. Additive Manufacturing: scientific and technological challenges, market uptakes and opportunities. Materials Today. Vol 21, p. 24-26

Uzun, G. Korkut, I. 2016. The effects of cutting conditions on the cutting torque and tool life in tapping process for AISI 304 stainless steel. Materials and technology. Vol 50, p. 277-278

Yamazaki, T. 2016. Development of a Hybrid Multi-tasking Machine Tool: Integration of Additive Manufacturing Technology with CNC Machining. Procedia CIRP. Vol 41, p. 82-84

Yilbas, B. Sahin, A. 2014. Friction Welding Thermal and Metallurgical Characteristics. Springer. SpringerBriefs in Applied Sciences and Technology, p. 1-2

What-when-how. 2019. [Web document] [Referred: 11.03.2019] Available: http://what-when-how.com/metrology/terminology-of-gear-tooth-metrology/

Zhang, B. Li, Y. Bai, Q. 2017. Defect Formation Mechanisms in Selective Laser Melting: A Review. Chinese Journal of Mechanical Engineering. Vol 30, p. 517-519

Zhou, M., Liu, W., Wu, H., Song, X., Chen, Y., Cheng, L., He, F., Chen, S., Wu, S. 2016. Preparation of a defect-free alumina cutting tool via additive manufacturing based on stereolithography – Optimization of the drying and binding processes. Ceramics International. Vol 42, p. 11598-11602

APPENDIX 1: M16 tap technical drawing

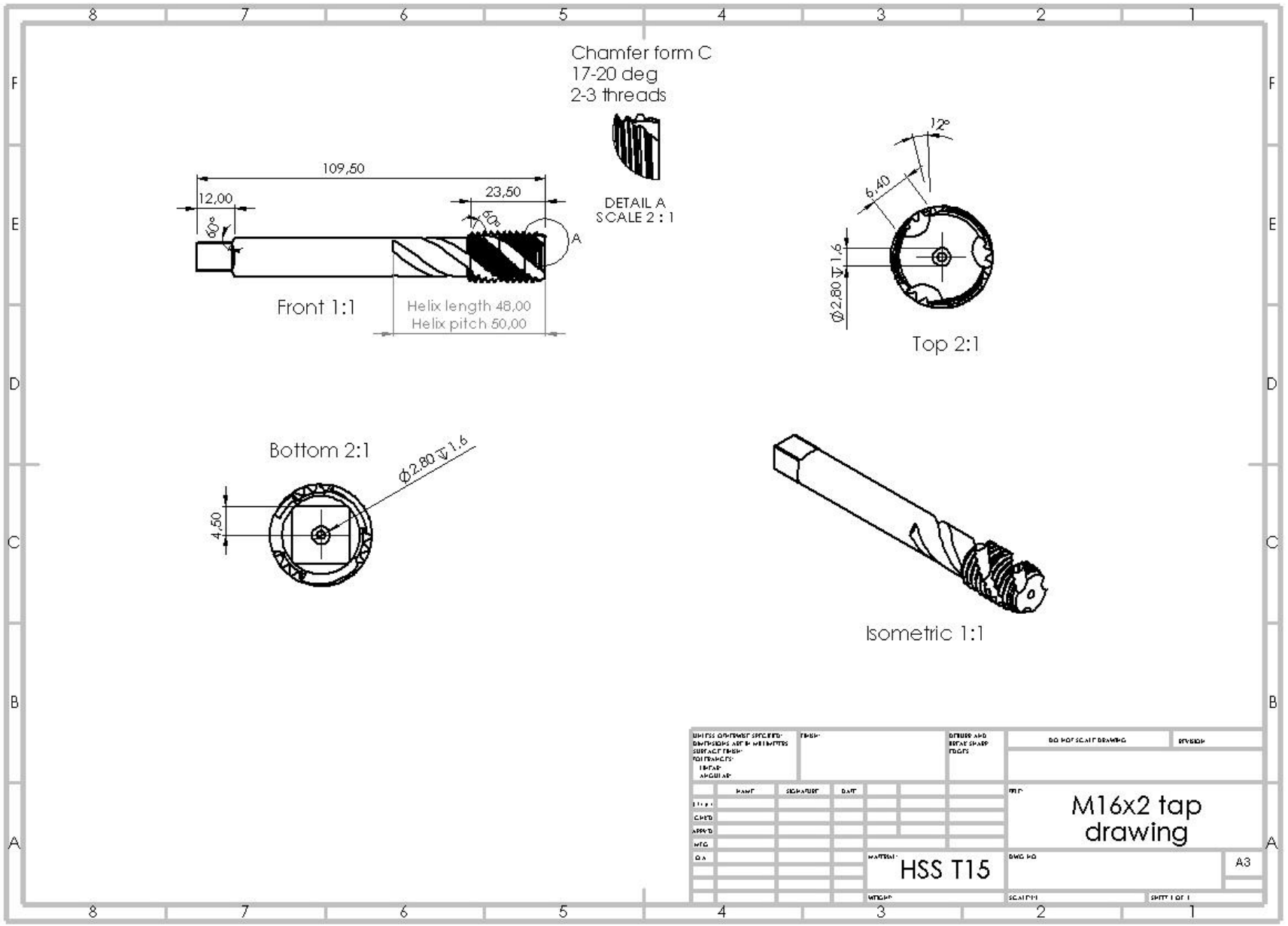

APPENDIX 2: Design study results for optimal chamfer angle

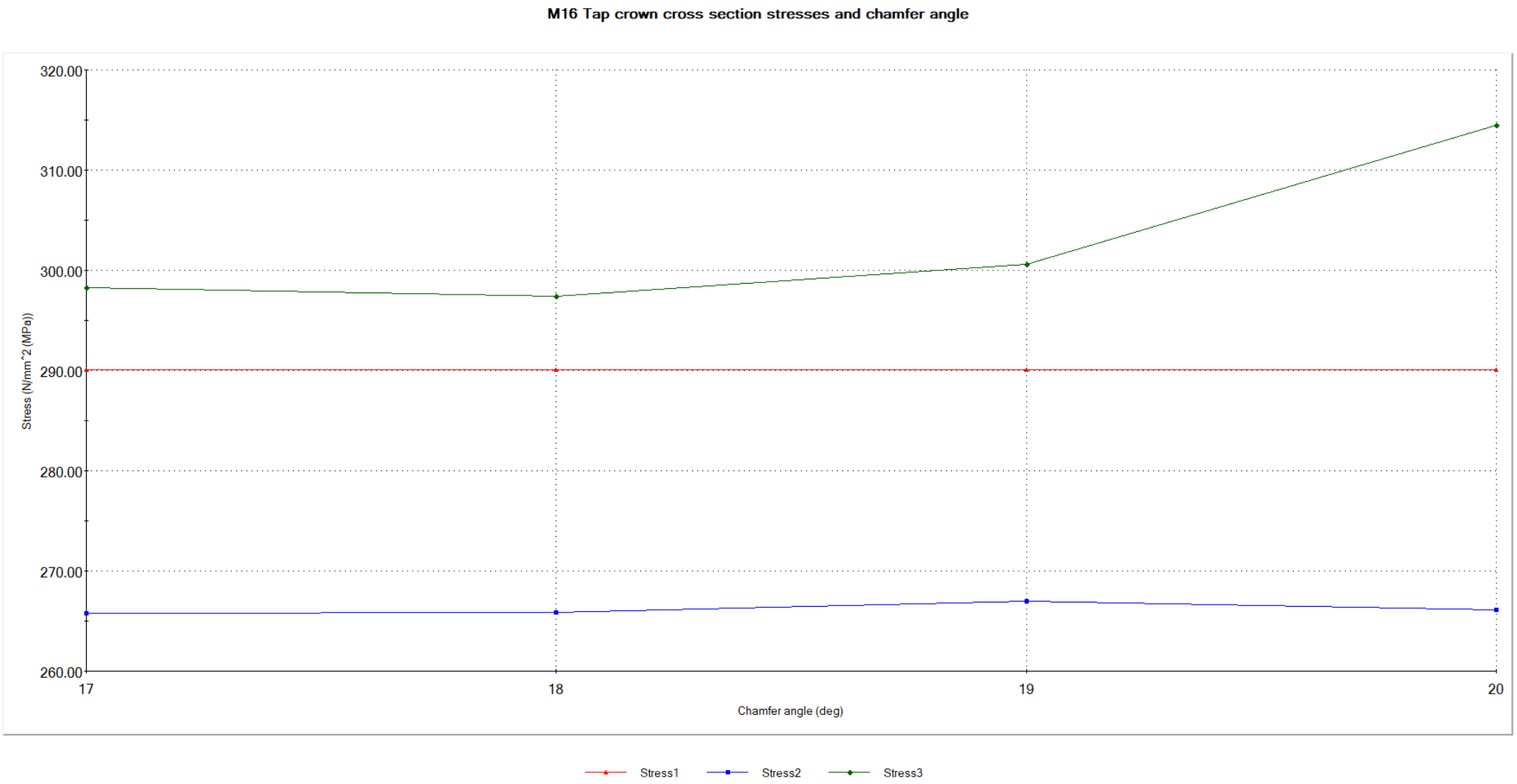

APPENDIX 3: Design study results for optimal chamfer length

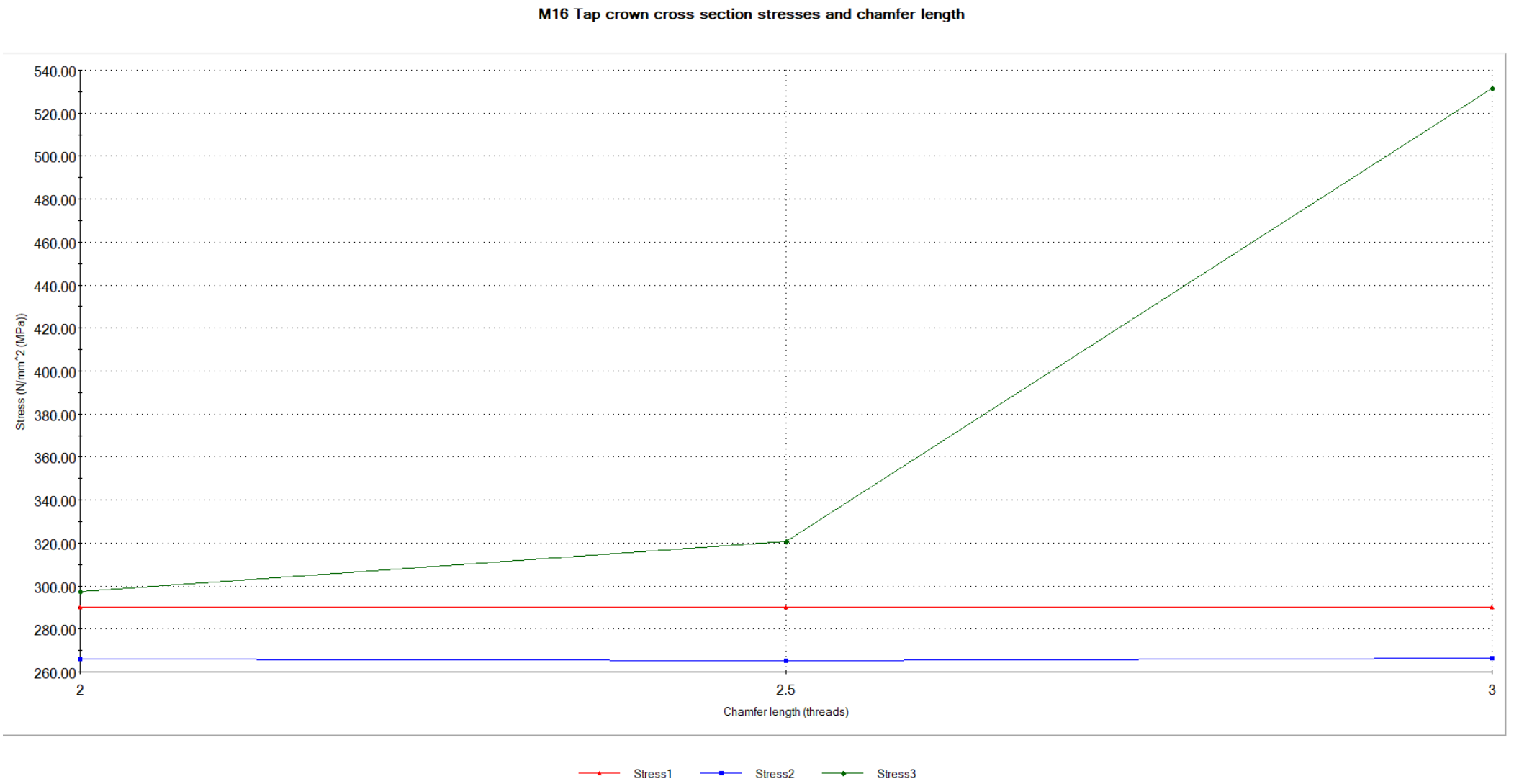

APPENDIX 4: Topology optimization results

M16x2 HSS T15 Configuration	Tap crown mass (g)	Crown mass reduction (%)	Stress1 (MPa)	Stress2 (MPa)	Stress3 (MPa)
Standard	27,22	0	301	274	299
Design optimized	27,31	0	290	266	297
Initial pentagon	22,63	17	342	341	345
Optimized pentagon	23,01	16	307	329	371
Initial square	24,31	11	331	318	316
Optimized square	23,96	12	306	312	349
Initial hexagon	21,44	21	366	355	379
Optimized hexagon	22,79	16	312	306	361
Initial hollow	15,1	44	1054	1249	804
Optimized hollow	19,14	30	388	724	534

APPENDIX 5: Tap crown print results

APPENDIX 6: Java script for tapping torque measurement

```
#include <HX711.h>

#define DOUT  3
#define CLK  2
#define GRAVITY 9.81

HX711 sensor;

float calibration_factor = -82000; // derived by calibrating the load cell with a known weight
float distance = 0.1; // 0.1 m for SS 0.125 m for Al

void setup() {
  // setup code, runs once:

  Serial.begin(9600); // Arduino data transmission rate
  sensor.begin(DOUT, CLK); // Arduino-HX711 pins
  sensor.set_scale(calibration_factor);
  sensor.tare(); // sets load cell scale to 0

  Serial.println("CLEARSHEET");
  Serial.println("CLEARDATA");

  Serial.println("LABEL,Time (ms),Torque (Nm)"); //names of the columns in excel

  Serial.println("RESETTIMER"); // sets time to 0
}

void loop() {
  // main code, runs repeatedly:

  float Reading = sensor.get_units()*GRAVITY; // Derives tapping force
```

```
  float Torque = Reading * distance; // Derives tapping torque

  Serial.print("DATA,");

  Serial.print(millis()); // time in milliseconds
  Serial.print(",");
  Serial.println(Torque);

  delay(500); //adds a delay of 0.5 s per output result

}
```